

# **Through the looking glass: using X-T plane distortions for wavefield separation**

David C. Henley and Joe Wong

## **ABSTRACT**

In exploration seismology, we record the response of the earth to various controlled seismic energy sources applied at or near the earth's surface. Since the earth is an imperfect elastic half-space, usually containing many internal boundaries and irregularities, the seismic response recorded at the surface consists of many different modes of wave propagation, some related to the surface of the half-space, others generated by the internal structure. Typically, we are primarily interested in using various back-scattered modes, like reflections, to construct images of the internal structure of the earth, so we need to separate one or more of these modes from the full seismic response for further processing. The separation is often accomplished using various mathematical transforms which take advantage of some unique characteristic of one or more of the modes.

In this work, we show how to apply some relatively simple geometric distortions to the X-T plane in which we usually display seismic data, to separate wavefield components for further processing. Since these distortions are all implemented as point-to-point re-mapping and interpolation in the plane, they can be reversed, with relative fidelity depending only upon the interpolation method. We thus avoid integral transforms, since these can exhibit undesirable artifacts related to the transform aperture, caused by operations applied in the transform domain, or caused by irregularities in the original data domain.

We use physical model data for our demonstrations. Hence, techniques which perform well on these data should be effective, as well, on actual seismic field data.

## **INTRODUCTION**

### **Purpose of mapping transforms**

A measured seismic wavefield as observed on a set of seismic field data generally consists of groups or ensembles of traces, or time records of elastic disturbances detected at discrete points on the earth's surface. On each ensemble, there is usually a pattern of recognizable 'events', or seismic waveforms whose geometric arrangement on the trace ensemble is characteristic of the type of event. Directly transmitted waves, for example, exhibit a linear pattern as a function of distance from the seismic source, while waves reflected from deep rock layer boundaries form a hyperbolic pattern. Since we typically wish to extract the reflection events for further processing into meaningful images of the subsurface rock layers, we use various geometric transformations of the input trace ensembles to enhance the reflections at the expense of all other events. The attraction of such transforms is their simplicity, the intuitive ease of observing their action on events in the X-T plane, and the ease with which they can generally be accurately inverted.

## Useful mapping transforms

Reflection seismic techniques have been developed over many years to enable exploration geophysicists to visualize the structure and rock properties of the interior of the earth. Initially, the refracted and reflected energy of compressional body waves was used, first for mapping reflecting boundaries, then later for imaging these boundaries. As technology matured, however, other components of the elastic wavefield, created either by buried impulsive sources or surface continuous wave sources, have been successfully used for mapping and imaging. In any case, however, in the absence of a comprehensive full elastic, full waveform inversion technique, we need to isolate whichever single elastic wavefield component we intend to use for imaging, so that waveforms due to other modes, which don't fit our current imaging constraints, are effectively removed from the data before further processing. Typically, this is done as part of the initial raw data processing step, where we call it 'coherent noise attenuation'—coherent noise in this setting being any organized wavefield component which is *not* part of the wavefield mode we're trying to image. Since we typically use singly reflected compressional waves for imaging, any other modes, like outgoing surface waves, guided waves, refracted waves, converted waves, and reflected shear waves are considered 'noise', and we attempt to remove them from the data before further processing. Similarly, if we desire to image singly reflected shear waves, or simple converted waves, we attenuate all other modes before proceeding to the imaging steps. Even if our intention is not to use the data for imaging, but for studies of reflection/conversion amplitude, we must attenuate as many interfering modes as possible to ensure the accuracy of the measurements.

Separation of wavefield components is usually done by noting what characteristics distinguish a desired component from others present in the same 2D data panel and extracting that component based on its characteristics. Waveform frequency content, event slope, event origin, and relative event timing can all be used to help in this discrimination process. Usually, however, a desired wavefield component and the 'undesirable' coherent events that constitute 'noise' are significantly overlapped or entangled in the original linear X-T domain in which they were recorded, and only limited success is possible in separating them in that domain. Ground roll is a good example. Although the waveforms exhibited by ground roll are generally much richer in low frequencies than reflection events, they share a significant portion of the seismic bandwidth, and ground roll events physically overlap significant portions of reflection events in a 'noise cone' centred on the shorter source-receiver distances. This means that low-cut filtering to attenuate ground roll will significantly impact the bandwidth of reflection events, even if the filtering is applied only in the region of the 'noise cone'.

Situations like the ground roll example, where wavefield components cannot be adequately separated in the original domain, lead us to seek other domains which provide better separation of wavefield characteristics. Various integral transforms like the f-k transform or the Tau-P transform can provide such separation for some wavefield components. For the Tau-P transform, separation is achieved on the basis of local event slope or 'slowness', P, and retarded time, Tau; this can lead to effective separation of simple multiple events from primary reflections, and the collapse of linear events into localized regions in the Tau-P domain, where they can be muted. The f-k transform, on the other hand, can separate events based on slope and bandwidth, and is most successful

at isolating events like refractions and repeated initials. A drawback of integral transforms, however, is that the transform must generally be applied to the entire input data array, and this array must generally be uniformly sampled. Furthermore, operations applied to data in these transform domains often lead to artifacts in the original  $X$ - $T$  domain.

### *NMO transform*

One type of domain that is often overlooked for wavefield separation is that which is involved in the general class of geometric transforms, or point-to-point mapping transforms. Mapping transforms are characterized by a simple formula or rule, which dictates where each point in an input data array must be placed in the new domain, as well as an interpolation operation to make the sample interval in the transform domain uniform. These transforms generally cause a recognizable geometric distortion of the original domain and can be inverted with great accuracy. The most familiar example is the normal moveout (NMO) operation, which maps each point in a seismic  $X$ - $T$  trace ensemble into a point in an  $X$ - $T_0$  ensemble and interpolates sample amplitudes as necessary to maintain uniform sampling in the  $T_0$  direction. The formula used for the mapping is the simple hyperbolic moveout formula,

$$T^2 = T_0^2 + \frac{X^2}{V^2(T_0)}, \quad (1)$$

where the NMO velocity in the formula is supplied as a uniformly sampled vector,  $V(T_0)$ . As can be seen from the formula, only the  $T$  coordinates of the input data samples are changed... $X$  remains unchanged. Hence, amplitudes posted at coordinates  $X$  and  $T$  in the input domain are posted unchanged at coordinates  $X$  and  $T_0$  in the transform domain, and any amplitudes required at unfilled  $T_0$  positions caused by the stretch of the transform are interpolated. When the interpolation is done properly, the NMO transform is exactly invertible...that is, the original  $X$ - $T$  array of input samples can be exactly recovered from the transformed  $X$ - $T_0$  array. Furthermore, the entire input array need not be involved in the forward or reverse transform, there are no artifacts created by a mapping transform, and the accuracy of the transform does not depend on what portion of an input array is involved. The NMO transform is an example of a geometric transform where the distortion of the input  $X$ - $T$  domain occurs parallel to the  $T$  axis—the  $X$  axis remains unaffected in sample position and increment. The most important characteristic of the NMO transform in terms of wavefield separation on an input seismic ensemble is that all events corresponding to the supplied RMS velocity function become linear and parallel to the  $X$  axis, while all others retain some slope.

### *RT transform*

Another example of a mapping transform where the distortion is confined to one dimension, in this case orthogonal to the  $T$  axis, is the Radial Trace (RT) Transform. This mapping is generated by the pair of relations:

$$T' = T - T_0, \quad (2)$$

$$V = \frac{X - X_0}{T - T_0}, \quad (3)$$

where  $V$  and  $T'$  are the coordinates of the RT domain, and  $T_0$  and  $X_0$  are the coordinates of the ‘origin’ of the mapping, which may or may not be zero (coincident with the origin of the original  $X$ - $T$  array). As can be seen, the  $T'$  coordinate is just a shifted mapping of the original  $T$  coordinate, retaining the same sample interval. The  $V$  formula, (3), however, determines a sloping trajectory in the  $X$ - $T$  plane along which amplitudes are sampled for the RT domain. Since many of the required RT sample values, dictated by the  $T'$  sample increment, will fall between the actual values of  $X$ , interpolation is required to create the missing amplitudes from posted ones. While any one of several interpolation methods can be applied, involving various sophisticated functions; one perfectly adequate method interpolates amplitudes orthogonal to the  $T'$  direction from the two nearest posted amplitude values at  $X$  sample positions. If the so-called ‘nearest neighbour’ interpolation is used, the resulting RT Transform is exactly invertible (as long as enough  $V$  trajectories are used to adequately sample the input  $X$ - $T$  array. A more useful two-point interpolation, however, is the so-called  $p$ -norm interpolation, where each interpolated amplitude consists of the weighted average of the two nearest input sample amplitudes at the same  $T'$ . Here, the weights are the reciprocals of the  $p$  power of the distance,  $l$ , to each input sample; and  $p = 1$  corresponds to linear interpolation. As  $p$  increases, the interpolated amplitude value increasingly favours whichever of the two input values is in closest proximity, until as  $p$  approaches  $\infty$ , the interpolation becomes ‘nearest neighbour’. As with any mapping transform, the transform need not be applied to the entire input array. Sometimes, it is useful to apply the transform to a velocity-defined wedge of an input trace ensemble. For wavefield separation, the RT transform is most useful because its choice of origin can be used to align its mapping trajectories with the wavefronts of various events in the wavefield. This alignment serves not only to confine the events to narrow regions of the RT domain, but also to shift the apparent bandwidth to very low frequencies, thus providing further separation (Henley, 2003, 2011a).

### $T^2$ - $X^2$ transform

A mapping transform in which distortion occurs in both dimensions is the  $T^2$ - $X^2$  transform:

$$T' = T^2, \quad (4)$$

$$X' = X^2, \quad (5)$$

where  $X$  and  $T$  are the original coordinates, and  $X'$  and  $T'$  are the coordinates in the new domain. Since this is a non-linear transform, interpolation is required in both dimensions to make the sampling uniform in the output  $T^2$ - $X^2$  domain. This domain is often used for velocity analysis, since the non-linear mapping linearizes any event with hyperbolic moveout, the linear slope being related to the NMO velocity of the event. While in theory, it is not necessary to map the entire  $X$ - $T$  plane, since it doesn’t affect the accuracy of the transform, in practice, there would be no reason not to map the entire domain.

*Interpolation and regularization*

Both the RT transform and the  $T^2$ - $X^2$  transform can be used to regularize seismic trace ensembles with uneven sampling in the  $X$  domain, since both will accept any values of  $X$  and interpolate them into the transform domain; whereupon inversion to the original  $X$ - $T$  domain will result in ensembles with uniform sampling in  $X$  (Henley, 2001). The nominal sample increment in  $X$  can be changed by the same mechanism, to implement simple two-point interpolation, which could be considered another point-to-point mapping transform, but with no distortion in either dimension.

*LMO transform*

A final useful mapping transform, which has no nonlinear distortion, requires minimal interpolation and is exactly invertible, is the linear moveout (LMO), or ‘vertical shear’ transform:

$$T' = T - \frac{X}{V}, \quad (6)$$

where  $V$  is a velocity parameter that determines the time shift applied to a trace at distance  $X$ . This mapping simply applies a vertical differential ‘shear’ to a trace ensemble, orthogonal to the  $X$  dimension, which makes any linear event with apparent velocity  $V$  orthogonal to  $T$ . The LMO transform is useful for removing or reducing the aliasing manifested by sloping events in the original  $X$ - $T$  plane, and it can be used in combination with simple interpolation to reduce the aliasing of those events when the LMO transform is reversed to yield the original  $X$ - $T$  domain (Henley, 2011b).

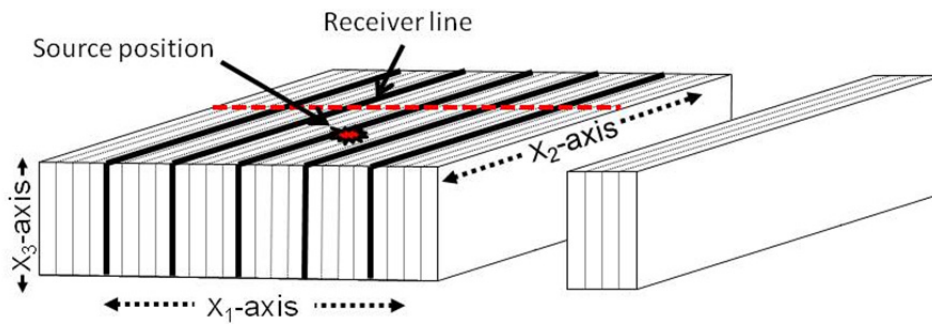
The transforms described above are only the most familiar examples of what we have termed mapping transforms—others can certainly be devised, related to the apparent geometry of seismic events on trace ensembles; but the ones above suit our current objectives. Also, the implementations of the above operations can vary considerably, particularly in the details of the embedded interpolation. The success of wavefield separation operations can depend somewhat on these details.

**Physical modeling**

We chose to use physical model data to demonstrate various wavefield separation operations based on mapping transforms for the following reasons:

- The recorded wavefield realistically imitates seismic field data in miniature, including realistic noise and attenuation.
- All the boundaries in the model are known, as are the elastic wave velocities of the model materials, unlike seismic field data.
- There is no near-surface layer to attenuate and distort the wavefield, once again, unlike seismic field data.
- Several clear wave modes are easily identifiable and can be individually targeted for separation.

The model chosen for analysis was a single layer consisting of five vertically oriented slabs of orthorhombic material cemented together (Mahmoudian et al, 2010, 2012a, 2012b) (Figure 1). The first seismic survey we studied (experiment 1) was a reflection survey performed along the top surface of the model, perpendicular to the strike of the cement seams, and the source was offset from the receiver line to simulate a 3D receiver line trace gather. The small-dimension piezoelectric transducers employed in the experiment are sensitive to particle displacements related to both shear and compressional wave motion. Hence, a wavefield exhibiting an abundance of coherent events was generated and recorded in this model experiment, as shown in Figures 2 and 3. In the next section, we show how to use various mapping transforms to extract desired events from the total recorded wavefield shown in Figures 2 and 3.



Layer composed of slabs of orthorhombic material (linen layers embedded in phenolic resin). The orientation of the receiver line and position of the source for the first experiment are shown.

FIG. 1. Schematic of the physical model used for demonstrating wavefield separation (after Mahmoudian et al)

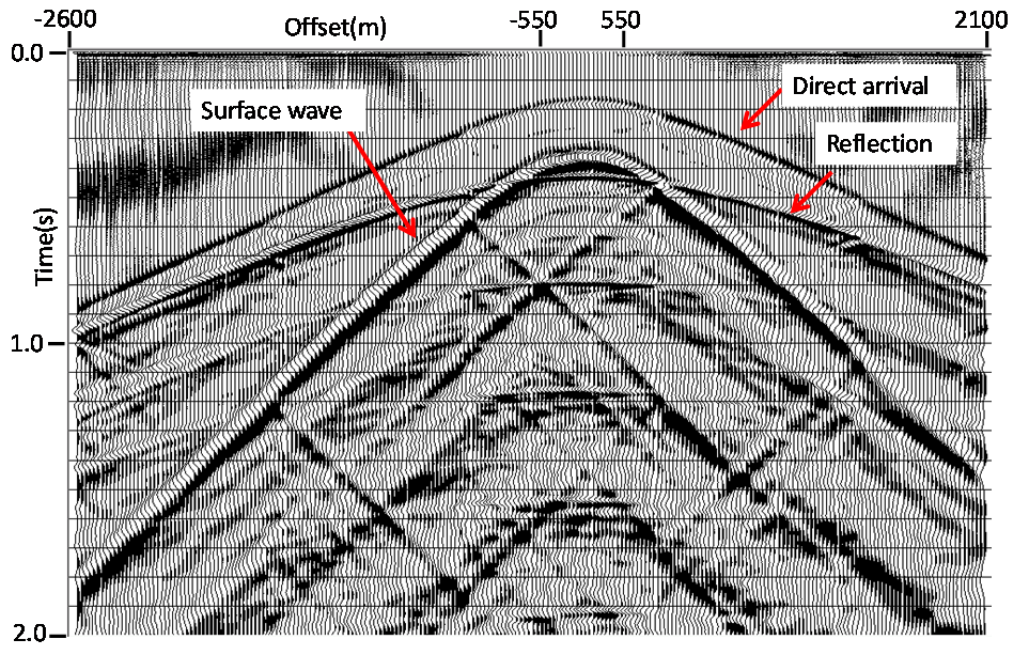


FIG. 2. Receiver line gather 1 acquired using the acquisition geometry shown in Figure 1. Note backscattered linear modes generated at the vertical seams of the model layer.

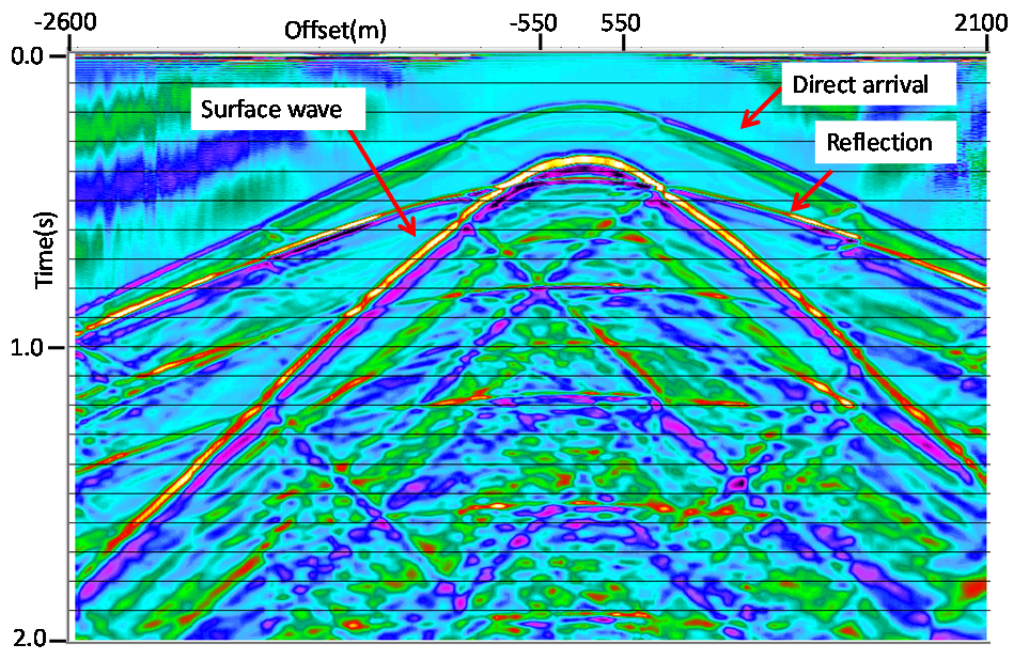


FIG. 3. Color version of Figure 2—receiver line gather 1 for physical model in Figure 1.

## EXPERIMENT 1

The objective for processing in this experiment was to obtain clean reflection responses whose relative amplitudes can be measured accurately for comparison with theoretical predictions. This means that significant portions of the target events must be relatively free from interference from other wavefield events. In all that follows,

unwanted events are always removed by modeling them and subtracting them. In this case, as long as the noise estimates do not significantly overlap target events in bandwidth *in the original domain*, the desired event amplitudes will be unaffected.

### Surface waves

On a 2D shot gather, surface waves are easily identified because of their linearity with source-receiver distance, as well as their origin at the source point. On a 3D receiver line gather, however, surface wavefronts assume a hyperbolic shape, just like reflections, with the apex opposite the source point. In this case, surface waves can be uniquely identified by mapping the source gather into the RT domain, as in Figure 4. Two different surface waves are identified by arrows in Figure 2, one the vertical component compressional wave, the other a radial component shear wave. These same surface waves are easily identified in Figure 4 as the vertically oriented events. Because these events are nearly parallel to the time direction, their apparent frequency is very low, making them easy to separate from the data and attenuate, using standard RT filtering methods (Henley 2003, 2011a).

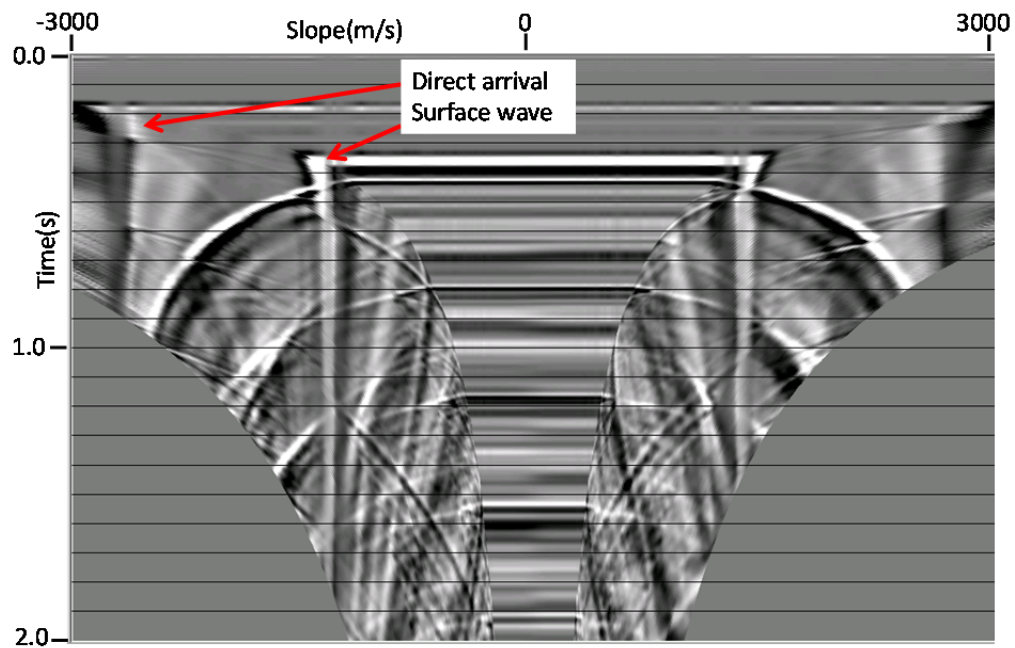


FIG. 4. Receiver line gather 1 in the radial trace (RT) domain. Surface waves whose moveout is linear with source-receiver offset become vertical, and therefore are very low in apparent frequency. Reflections and other events of interest retain higher frequencies.

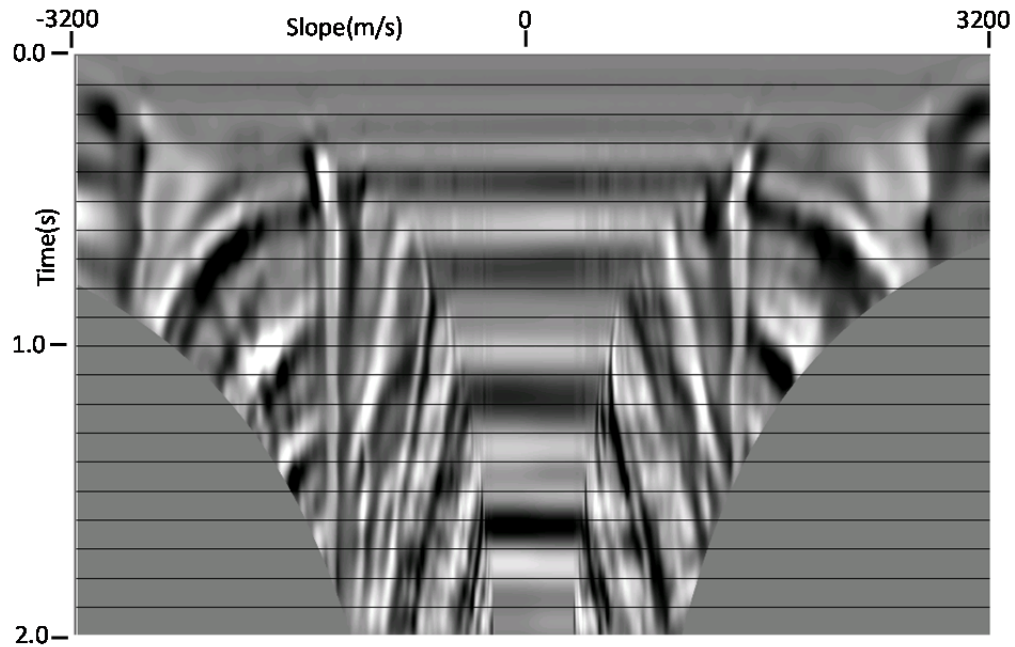


FIG. 5. Low pass filter removes reflections and other events, leaving mostly near-vertical low-frequency events. The inverse RT transform converts this to the  $X$ - $T$  domain surface wave estimate in Figure 6.

When we apply a low pass filter to the traces in Figure 4, we obtain the result in Figure 5. Note that most of the higher-frequency reflections and other hyperbolic events have been eliminated. Transforming this panel back to the  $X$ - $T$  domain, we get the surface wave estimate in Figure 6; and subtracting this from the original gather, we get results shown in Figures 7 and 8, the original 3D receiver line gather with most of the surface wave removed. In comparison with Figures 2 and 3, various hyperbolic events are much more prominent, as are numerous linear modes scattered from the 4 seams which join the five orthorhombic blocks of the model. Figure 9 is the RT transform of the filtered gather, and it confirms, in comparison with Figure 4, that the vertical, low-frequency modes associated with surface waves have been very effectively removed by the RT estimate-and-subtract technique demonstrated above.

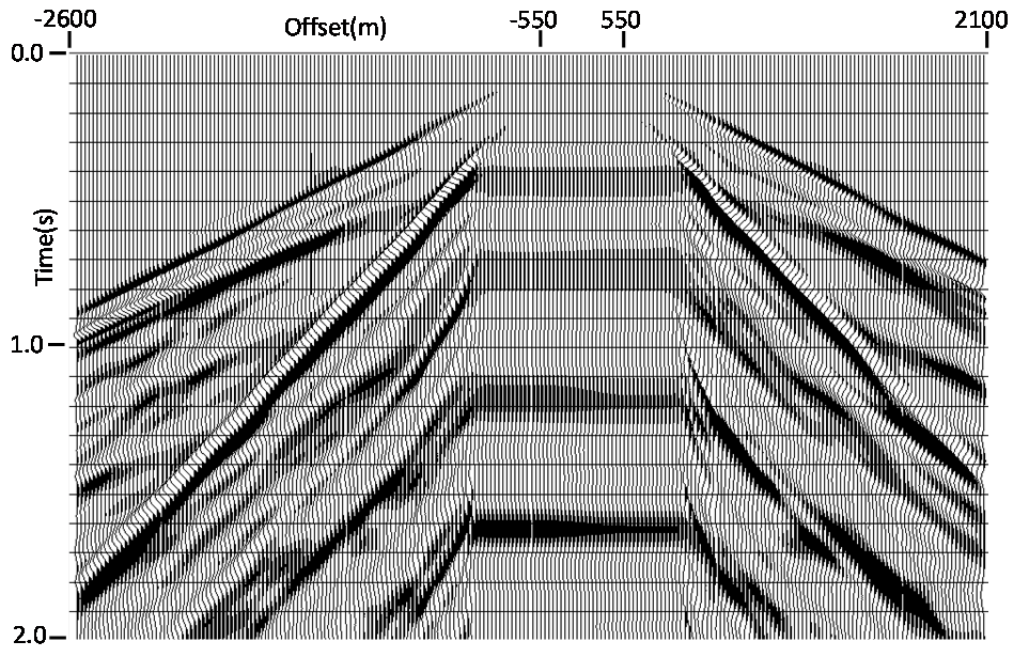


FIG. 6. X-T surface wave estimate provided by inverse RT transform of Figure 5.

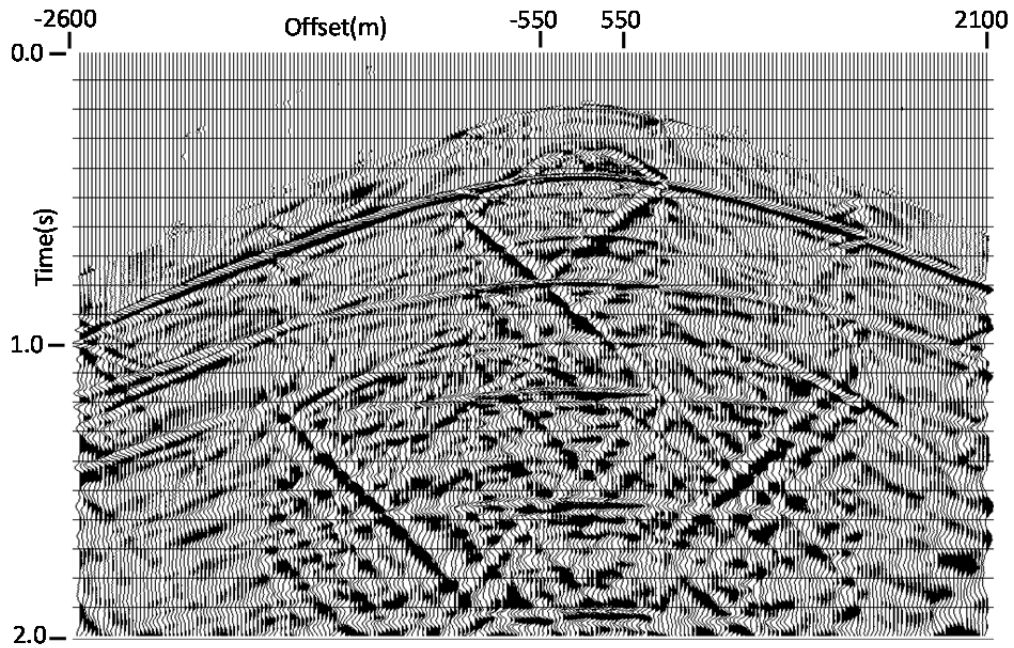


FIG. 7. Surface wave estimate of Figure 6 subtracted from Figure 2. Note the linear wave modes scattered from the 4 internal vertical seams in the model.

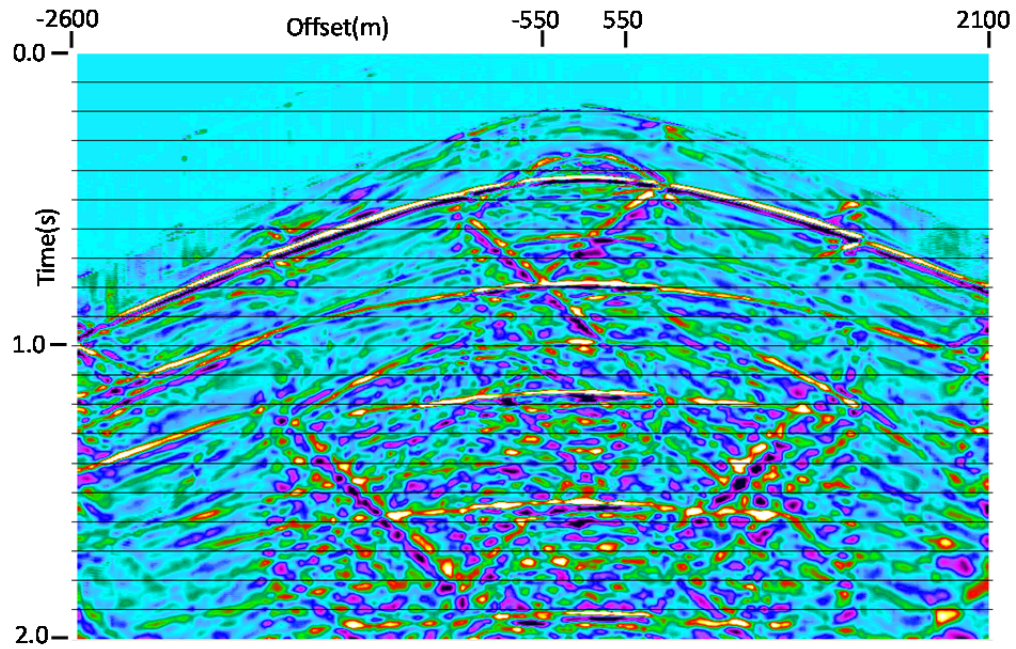


FIG. 8. Receiver line gather of Figure 7 in colour.

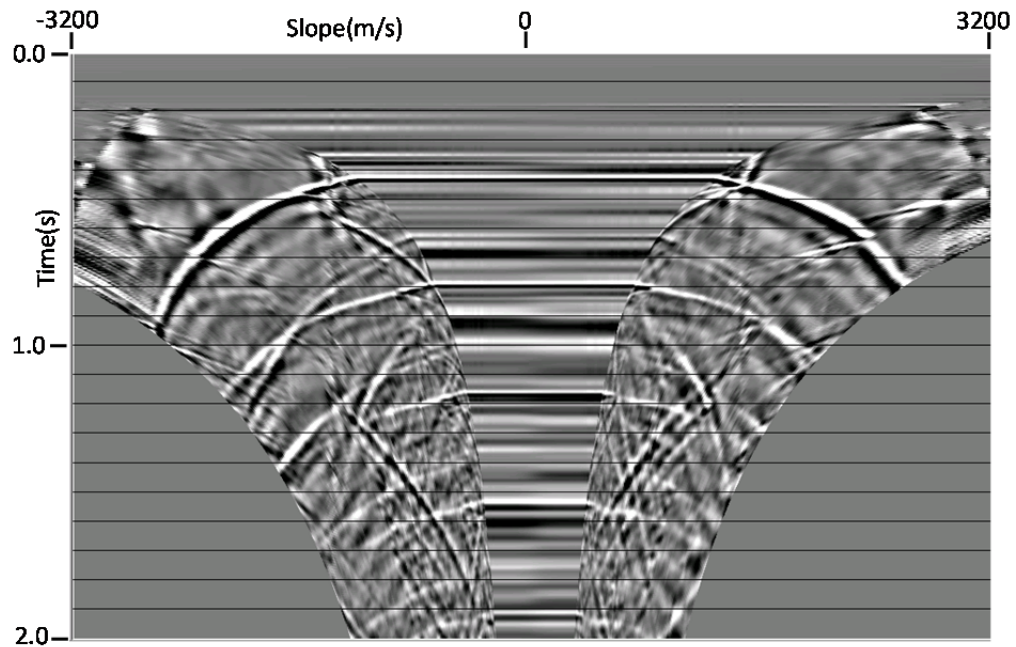


FIG. 9. RT transform of Figure 7, showing that the 'vertical', low-frequency modes are no longer present.

### Scattered linear modes

From past experience, we know that the kinds of linear modes observed in Figures 7 and 8 can be removed using RT filtering methods, where we employ RT 'dip' filters (narrow fan filters covering a small range of velocity) to target each distinct apparent velocity displayed by the linear events (Henley 2011a). After the application of a series

of RT dip filters, the receiver line gather is displayed in Figure 10, where we can now see at least two families of hyperbolic events, likely a PP primary reflection and its simple multiples, and an SS primary reflection and its multiples. A likely PS converted mode wavefront can also be seen. While there are a few fragmentary linear events still present in this gather, their dip is similar enough to that of the limbs of various hyperbolic events on the record that attempts to attenuate them would adversely impact the hyperbolic events as well.

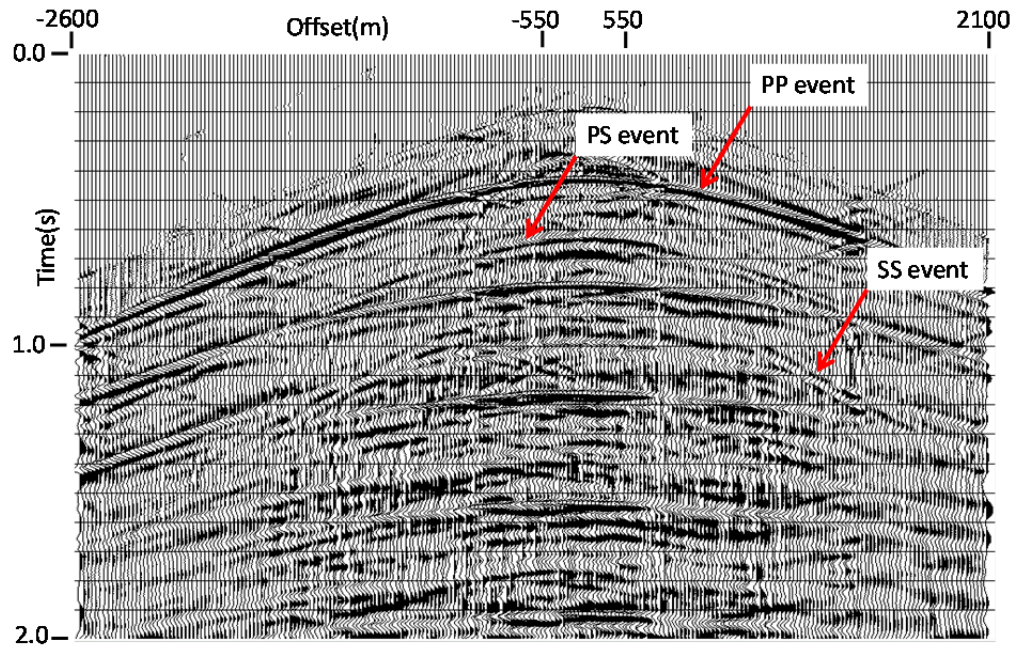


FIG. 10. Backscatter modes removed from receiver line gather 1 (Figure 7) using RT domain dip filters.

### Separating hyperbolic modes

A number of methods exist for separating seismic events with hyperbolic moveout, but we demonstrate one here which uses another of the mapping transforms described earlier: the  $T^2-X^2$  transform. The main characteristic of this transform is that all events with hyperbolic moveout become linear in the new domain. An important practical processing point to remember is that, even though the trace ensemble data are re-sampled in this transform, trace headers in the new domain must be re-built in a separate operation, since new traces are created. Figure 11 shows the  $T^2-X^2$  transform of the gather in Figure 10. The hyperbolic events have transformed to nearly linear events, which can be distinguished by their slopes. This makes it easy to apply RT dip filters to extract the desired family of events; Figure 12 shows the gather of Figure 10 after the slower events have been attenuated with RT dip filters, leaving only the PP primary reflection and its multiples. When we invert the  $T^2-X^2$  transform, the resulting gather, in Figures 13 and 14, contains primarily the PP reflection and its simple multiples—the PS and SS modes have been largely attenuated. In this particular implementation of the  $T^2-X^2$  transform, the output offset values are sparsely sampled in the near offsets in the forward transform, and must be interpolated in the inverse transform, the effect of which is visible in Figures 13 and 14.

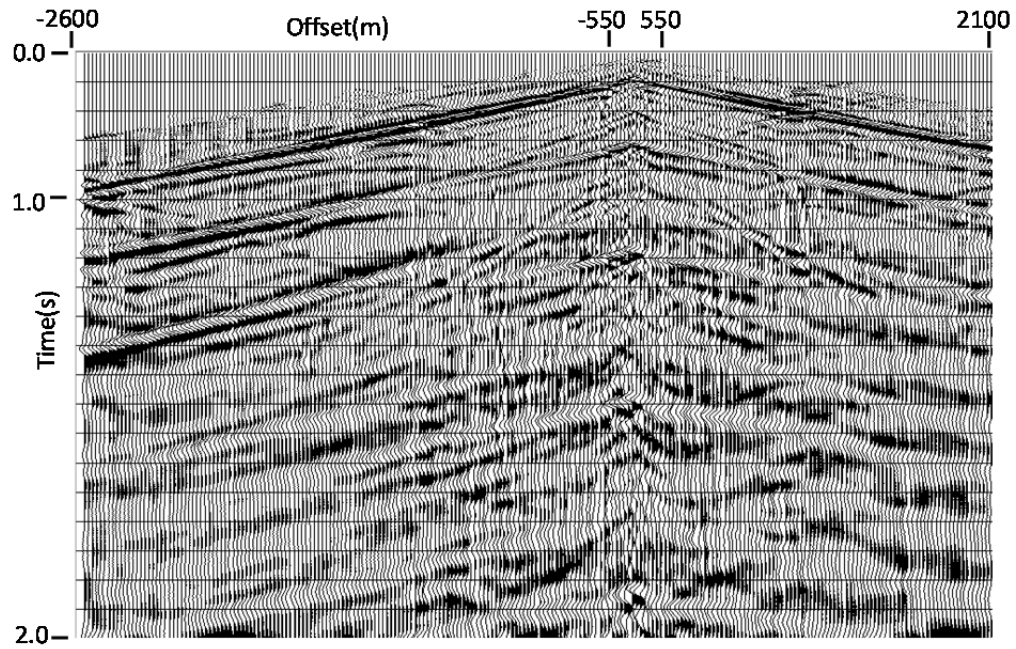


FIG. 11. Receiver line gather 1 in Figure 10 mapped to  $T^2$ - $X^2$  space. Events which were hyperbolic in  $X$ - $T$  space become nearly linear, making them easier to separate.

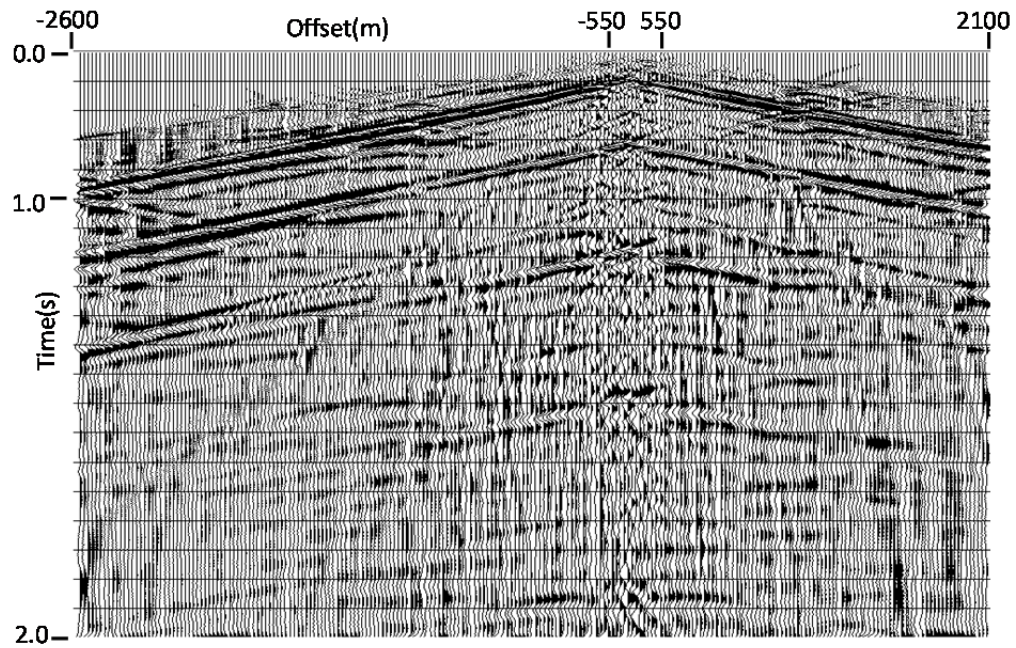


FIG. 12. Trace gather in Figure 11 filtered with RT dip filters to remove linear modes with lower apparent velocity.

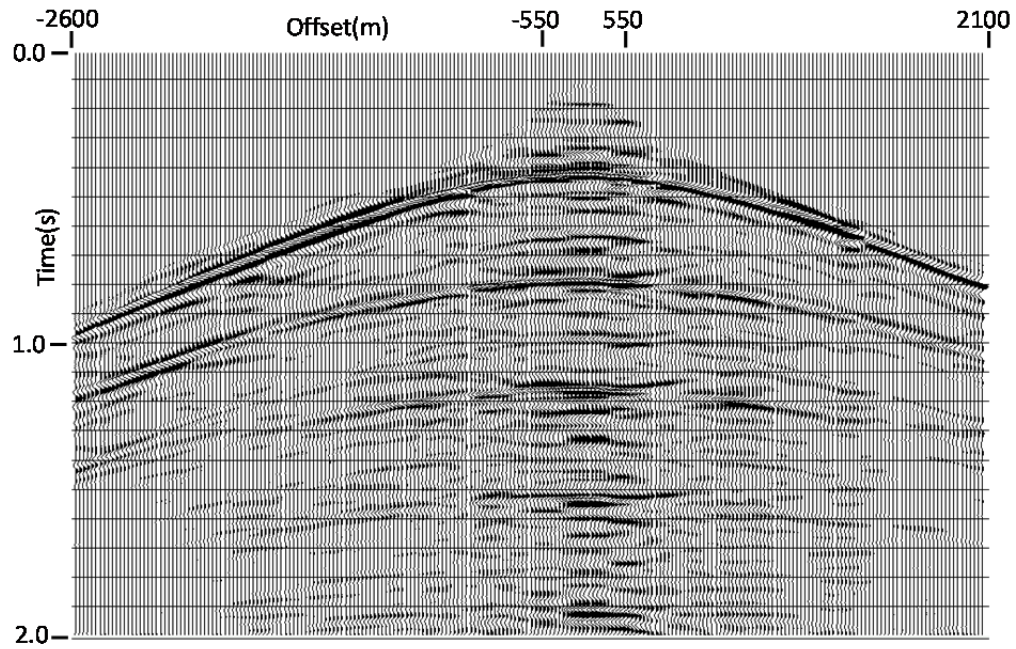


FIG. 13. Receiver line gather 1 after inverting  $T^2-X^2$  mapping to  $X-T$ . Several more low-velocity modes were subsequently removed by RT dip filtering. Most visible event energy is the PP event and its multiples. Most of the energy in linear, SS, and PS modes has been attenuated.

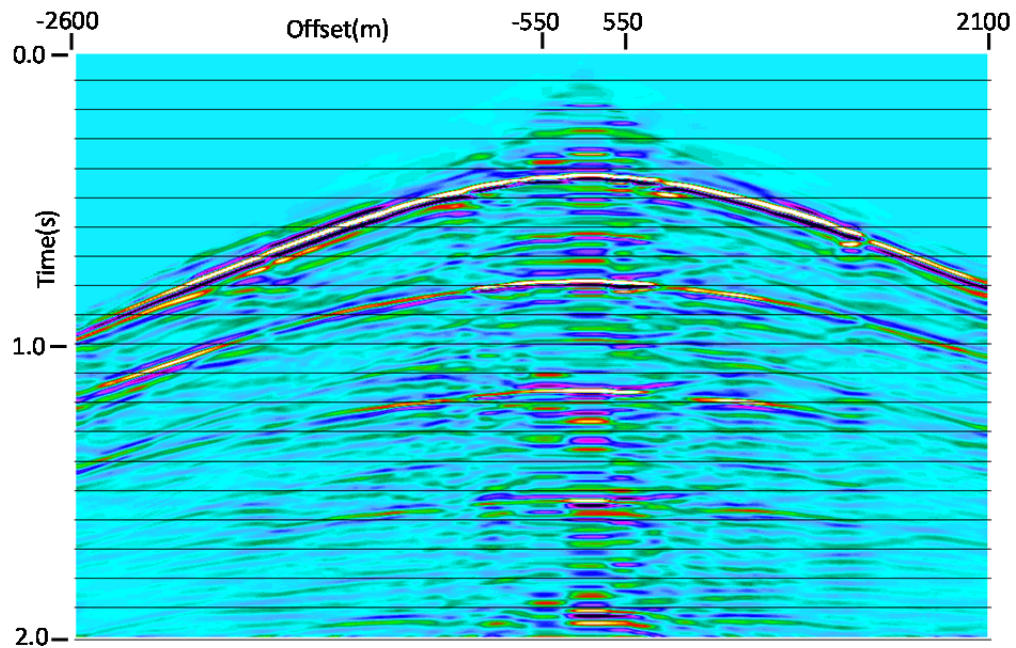


FIG. 14. Colour version of Figure 13.

If, on the  $T^2-X^2$  transform of Figure 11, we had applied RT dip filters to attenuate instead the PP reflection and its multiples, as well as the SS reflection, the inverse  $T^2-X^2$  transform would yield Figures 15 and 16, on which the PS event is particularly enhanced. As can be seen, the wavefield separation is not as complete as for the PP reflection, but

the PS event has been considerably enhanced and can be easily followed to quite large offsets before being obscured by interfering events.

Likewise, had we processed the original  $T^2-X^2$  transform with RT dip filters which suppressed the PP and PS modes, we could observe the enhanced SS event, as in the inverse  $T^2-X^2$  transform shown in Figures 17 and 18. In this case, the wavefield separation is even less complete, but the SS event is nevertheless enhanced enough to be useful for further analysis or processing.

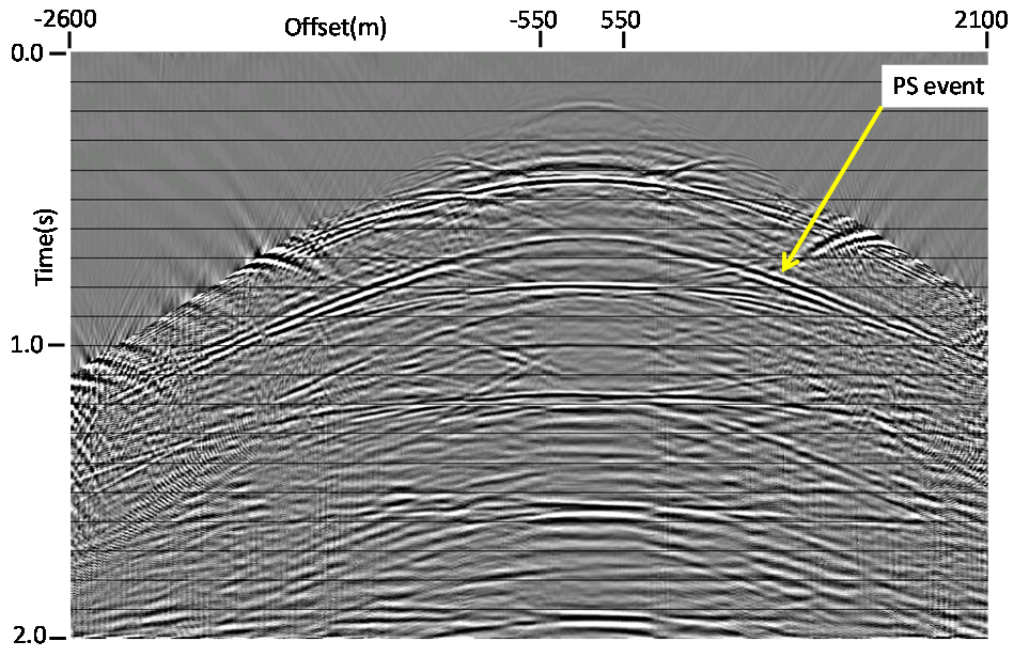


FIG. 15. Receiver line gather 1 processed to enhance PS primary event, instead of PP. Wavefield separation is not as complete as for PP, but the event is still usefully enhanced, and its amplitudes and arrival times could be measured, if desired.

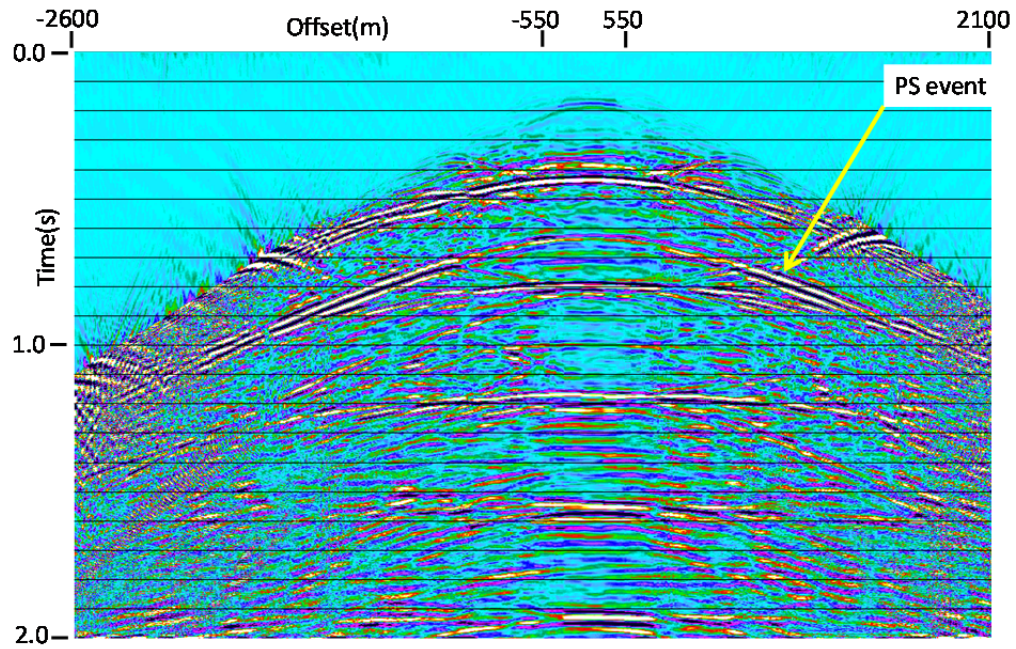


FIG. 16. Colour version of Figure 15.

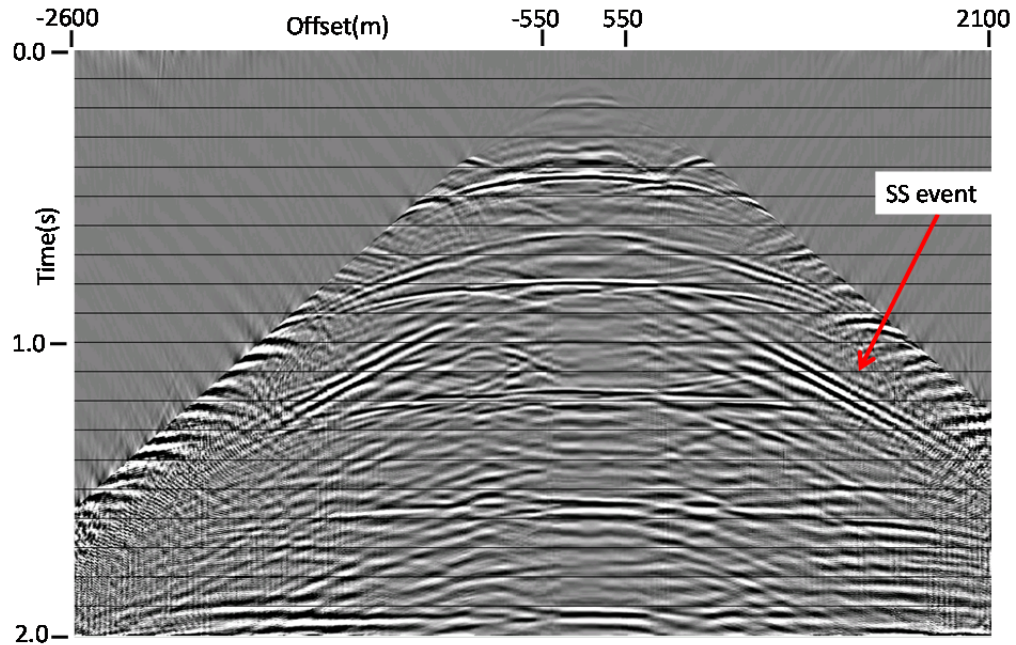


FIG. 17. Receiver line gather 1 processed to enhance SS primary event instead of PP or PS. The wavefield separation is even less complete than for PS, but the SS event is still enhanced enough for analysis.

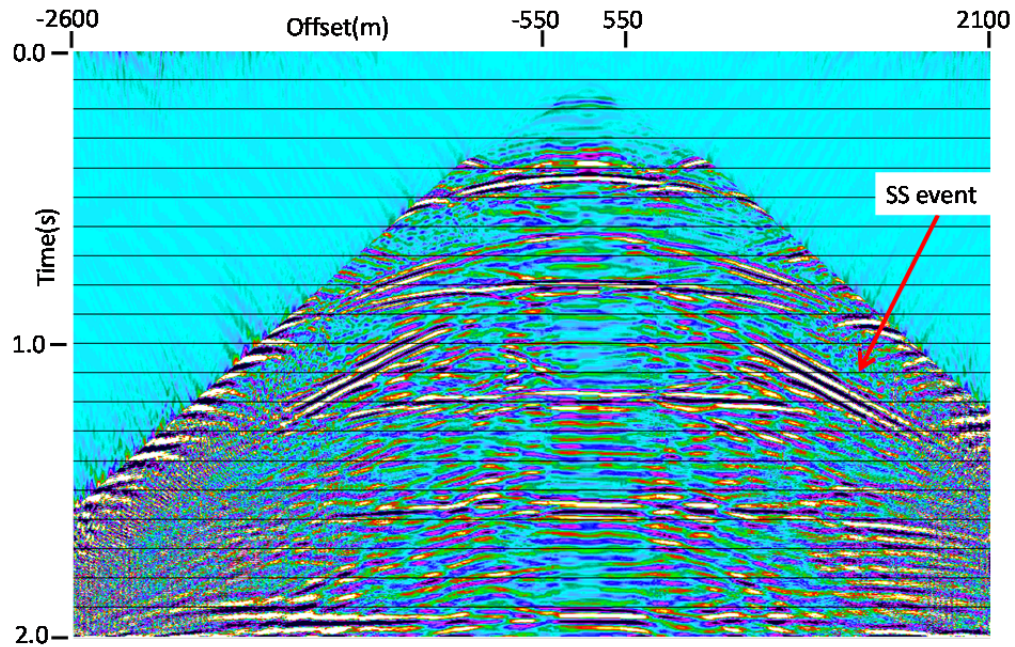


FIG. 18. Colour version of Figure 17.

To further illustrate, we processed a second receiver line gather from the same 3D survey. Figure 19 shows the raw gather, and Figure 20 shows the same gather after attenuation of the surface waves. Note that the linear modes scattering from the vertical seams in the model are stronger relative to the reflections than those we observed for the first receiver line gather in Figures 7 and 8. This is possibly due to the increased distance from the source to the receiver line. Nevertheless, these modes can be quite successfully removed, as shown in Figure 21. Comparing this gather with the first receiver line, we note a higher level of trace-to-trace fluctuations and high frequency noise. One way to suppress these effects is to apply a simple linear interpolation via the RT transform (Henley 2001). When we apply such an interpolation with an expansion factor of 4, the gather in Figure 22 is the result. If we then apply the  $T^2-X^2$  transform, Figure 23 is the result. On this gather, in addition to the quasi-linear events representing the reflections of interest, we also observe several groups of very steeply dipping linear modes. We can suppress these with the usual application of appropriate RT dip filters, at the same time that we do the hyperbolic mode separation, and the result is shown in Figure 24. Inverting the  $T^2-X^2$  transform, we get the gather in Figure 25, on which we can see yet more steeply-dipping noise at the shorter offsets. This can be removed as in Figures 26 and 27.

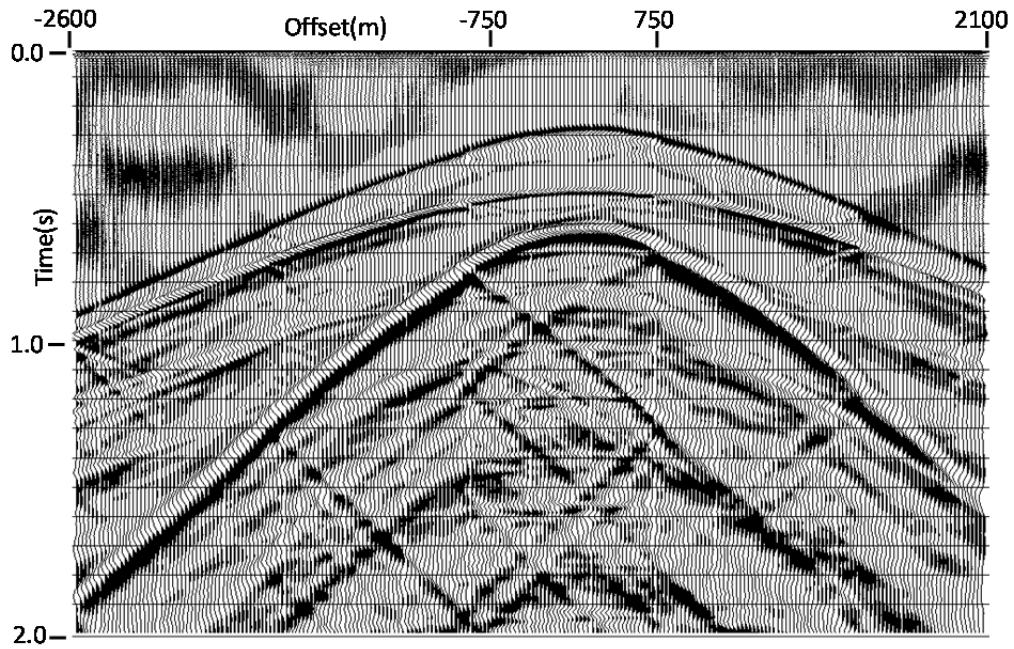


FIG. 19. Receiver line gather 2 from the 3D reflection survey of the model in Figure 1. The offset of source from receiver line is greater than for receiver line 1.

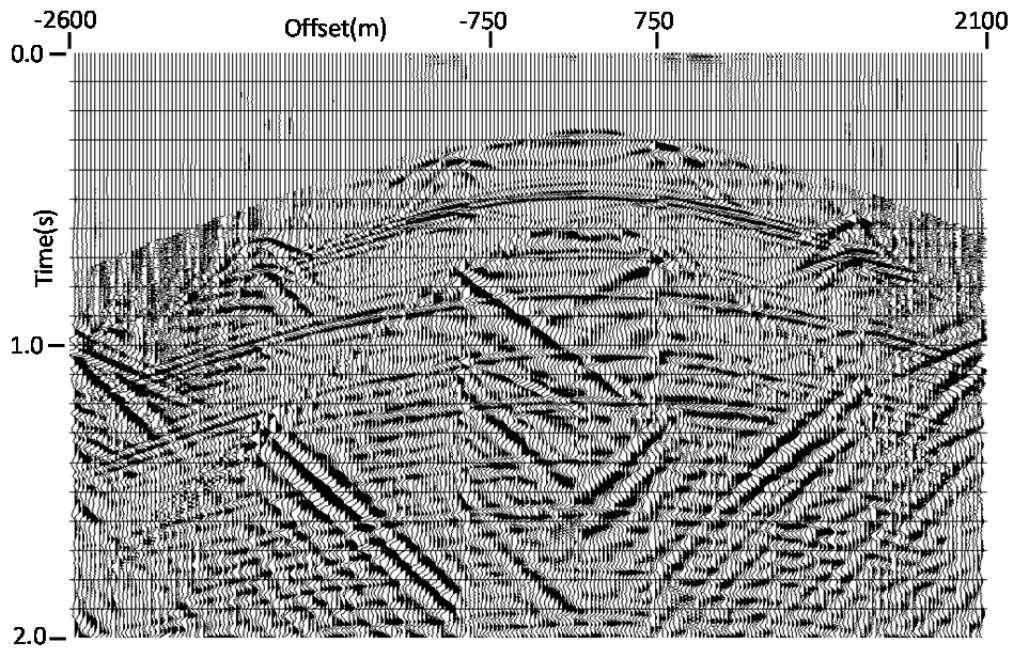


FIG. 20. Receiver line gather 2 after removal of the surface waves. Scattered linear modes are stronger, likely due to increased source-receiver line offset for this gather compared to gather 1.

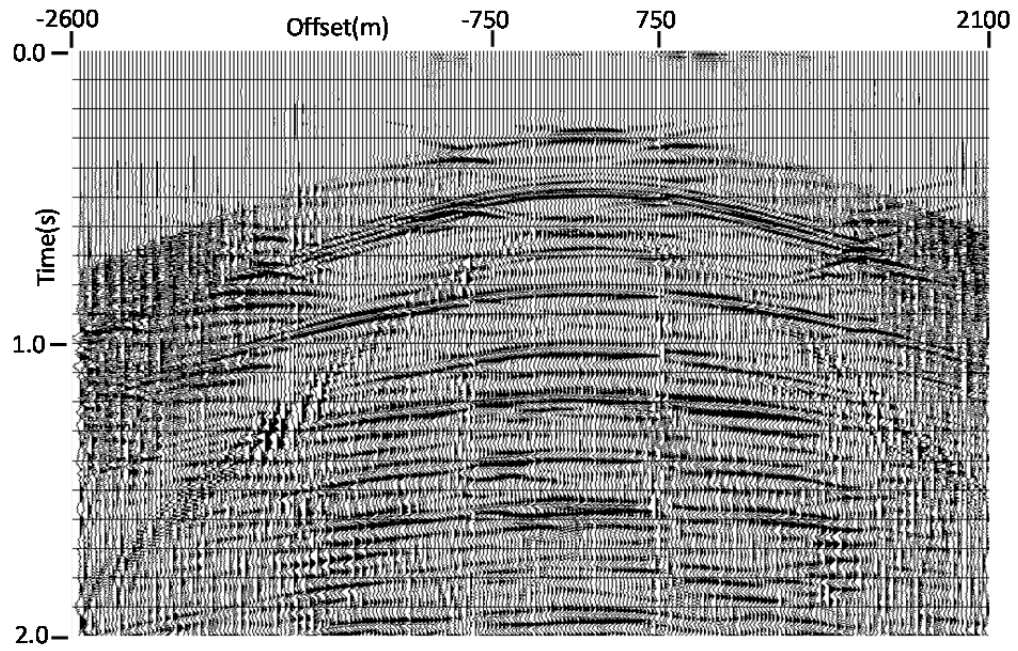


FIG. 21. Backscattered linear modes removed.

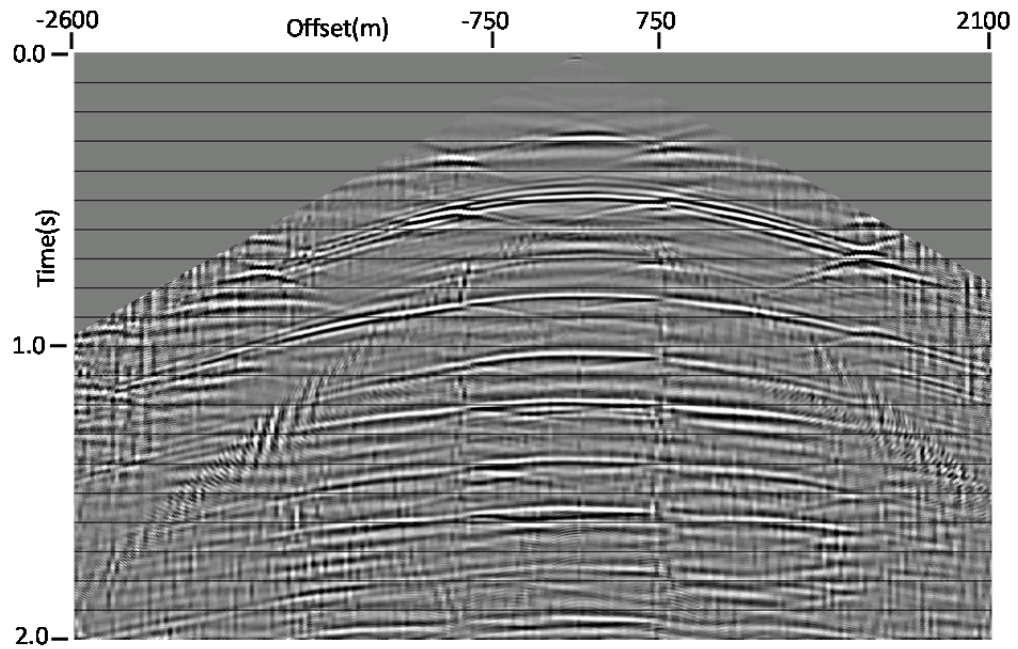


FIG. 22. Receiver line gather 2 interpolated x4.

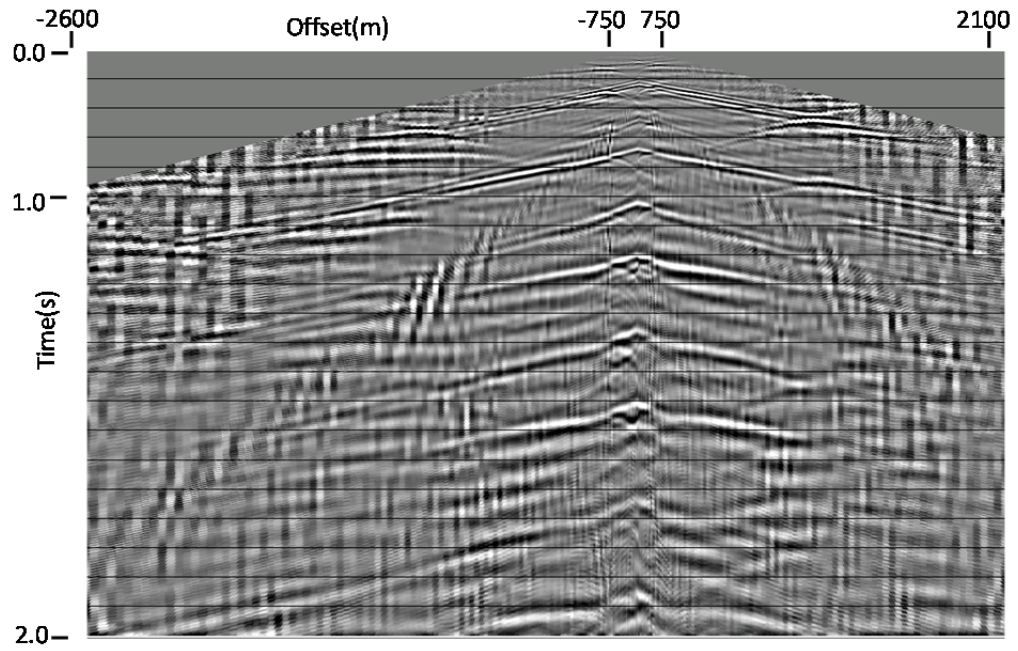


FIG. 23. Receiver line gather mapped to  $T^2-X^2$  space to linearize hyperbolic modes.

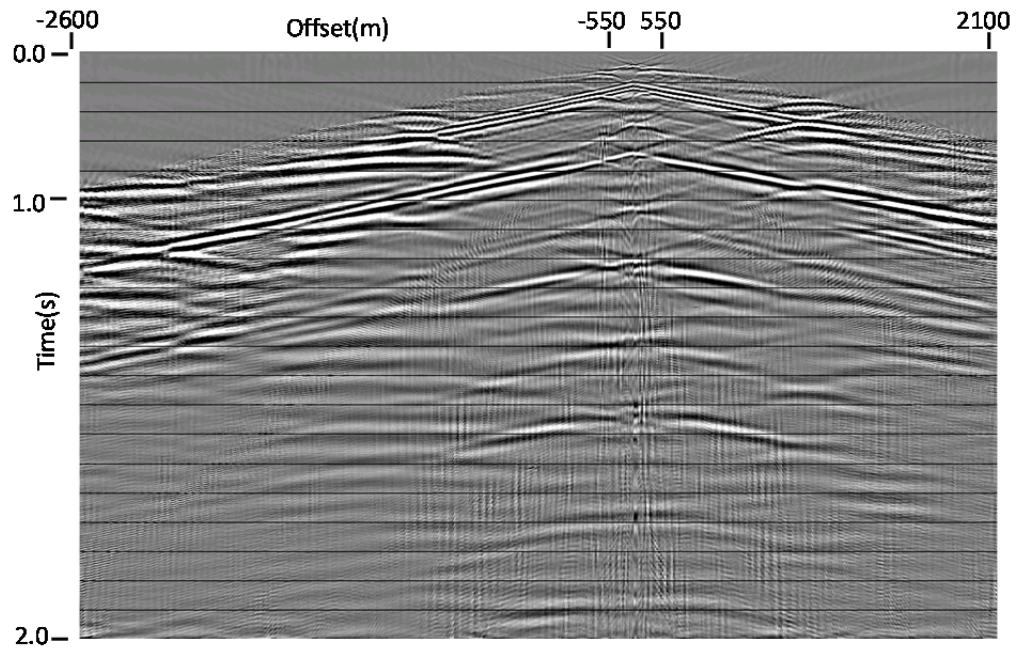


FIG. 24. Steep linear modes suppressed by RT dip filters.

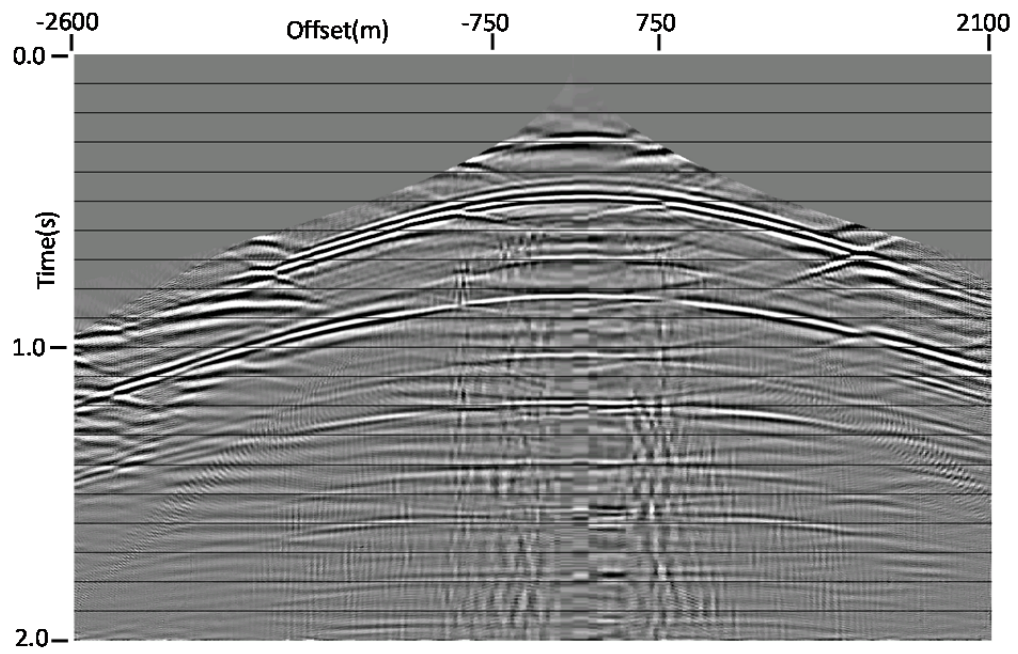


FIG. 25. Receiver line gather 2 mapped back into X-T domain.

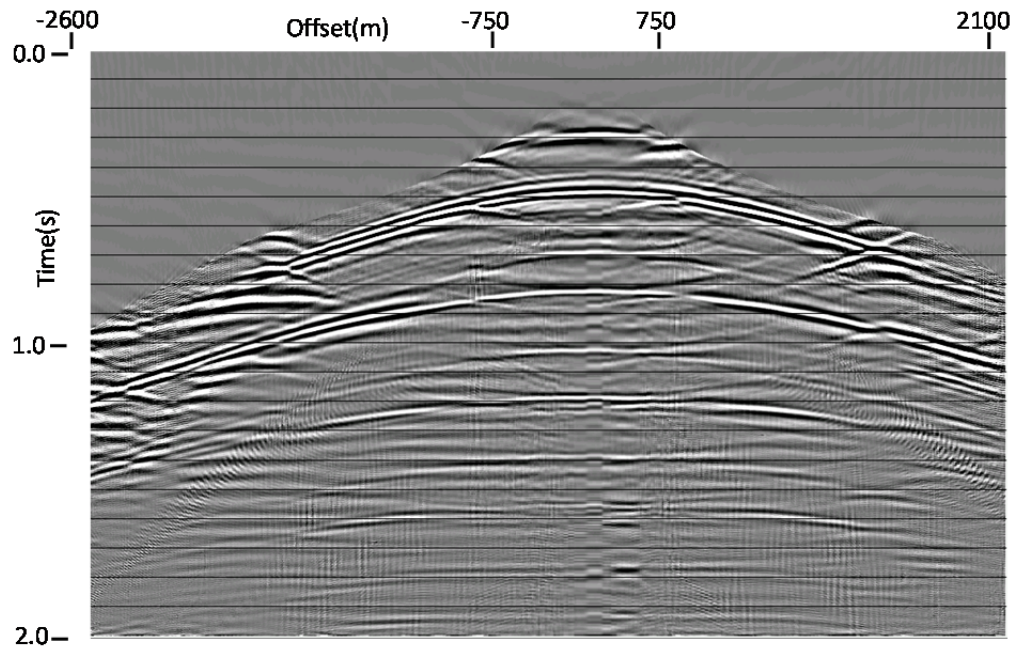


FIG. 26. More steep linear modes subtracted.

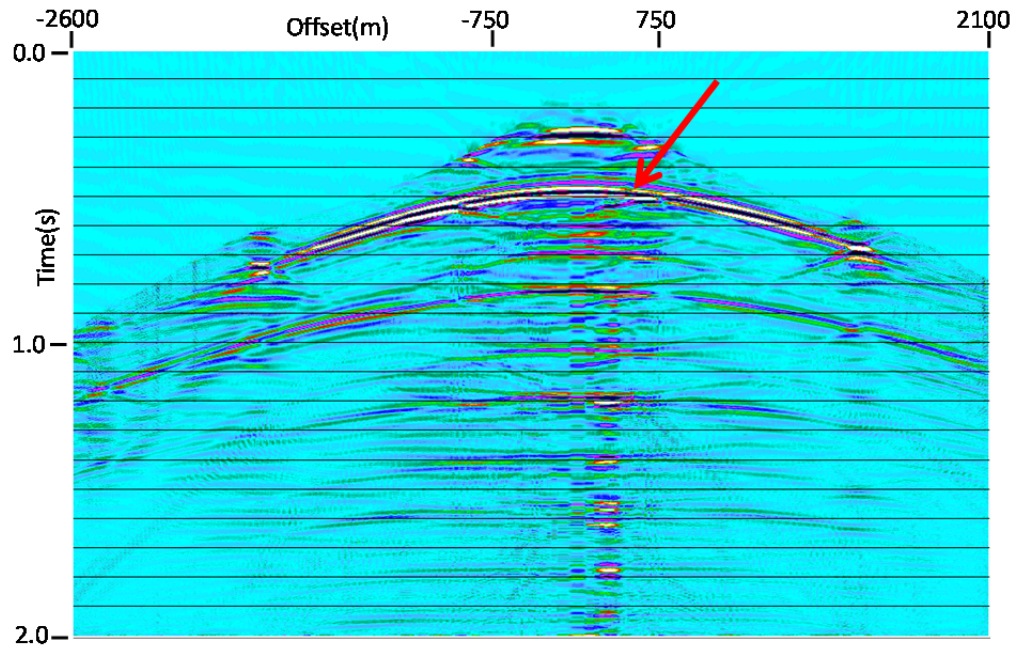


FIG. 27. Colour version of Figure 26—desired PP event highlighted.

## EXPERIMENT 2

In another separate demonstration of the use of simple mapping transforms in wavefield separation, we processed the wavefield recorded in a *transmission* seismic physical modeling experiment, which used the same orthorhombic physical model described above (Mahmoudian et al, 2012a, 2012b). In this case, instead of recording a 3D reflection survey with approximately single-point sources and receivers, all located on the upper surface of the model, much larger transducers were placed on opposite surfaces (upper and lower) of the model, and vertical, radial, and transverse displacements were recorded along a number of profiles oriented at various angles to the seams (and thus to the orthorhombic symmetry axis) of the model. We illustrate here the processing of one of the components (radial) along a profile perpendicular to the seams of the model (the same orientation as the receiver lines processed for experiment 1. The objective of this transmission experiment is different from that of the reflection experiment in that the target events simply need to be clean enough to pick their arrival times accurately. Event amplitudes are not the main objective of this experiment, but the wavefield separation described below is still based on estimation and subtraction and should, nevertheless, result in relatively accurate amplitudes.

Figure 28 shows a radial component trace gather from the transmission experiment. It is immediately apparent that mode leakage from the vertical component and scattered modes from the model seams contaminate the data enough to make accurate arrival picking very difficult for the target event (arrow). Because of the relatively coarse trace spacing on this gather, the target event is nearly aliased. Hence, in order to preserve this event properly, we adopt a slightly different approach to isolating it.

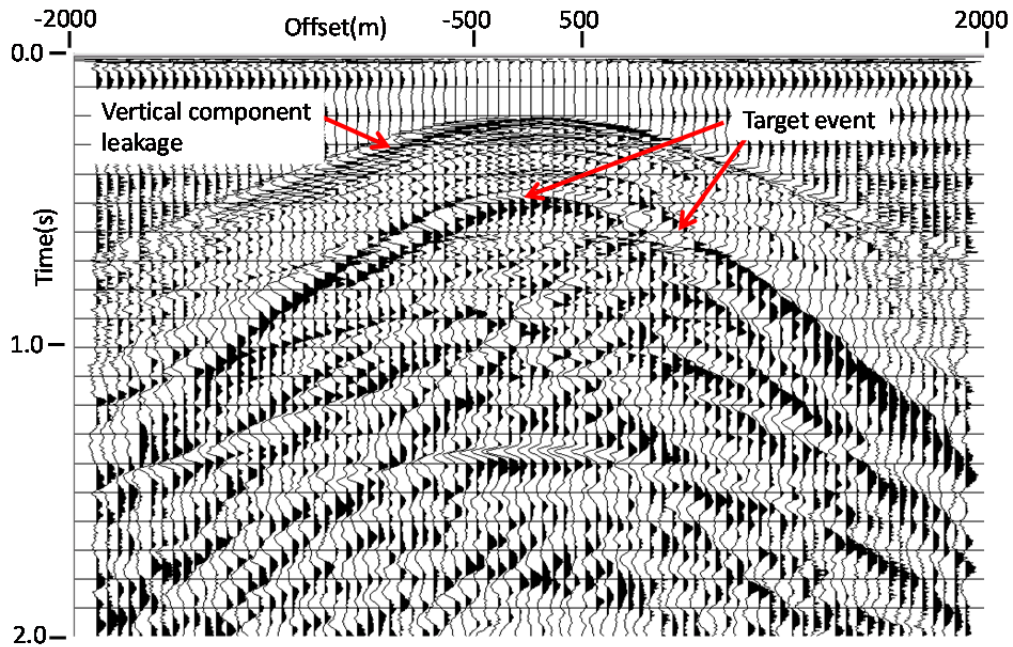


FIG. 28. Raw radial component source gather from transmission survey of model in Figure 1.

### Reducing the event alias

This data set is one instance where we can fruitfully apply the NMO transform, using the hyperbolic NMO velocity of the target event (1530m/s). For our purposes, we suppressed any stretch muting in the NMO algorithm and extended the traces by 300ms in order to capture as much as possible of the transformed wavefield. This helps to ensure the fidelity of the transform and its inverse. In Figure 29, the radial component gather has been transformed, and the only events now exhibiting aliasing are those whose NMO is significantly different from that of the target event, which is now almost perfectly flat. We next interpolated the traces by a factor of two to further reduce alias for the next step. This interpolation is shown in Figure 30.

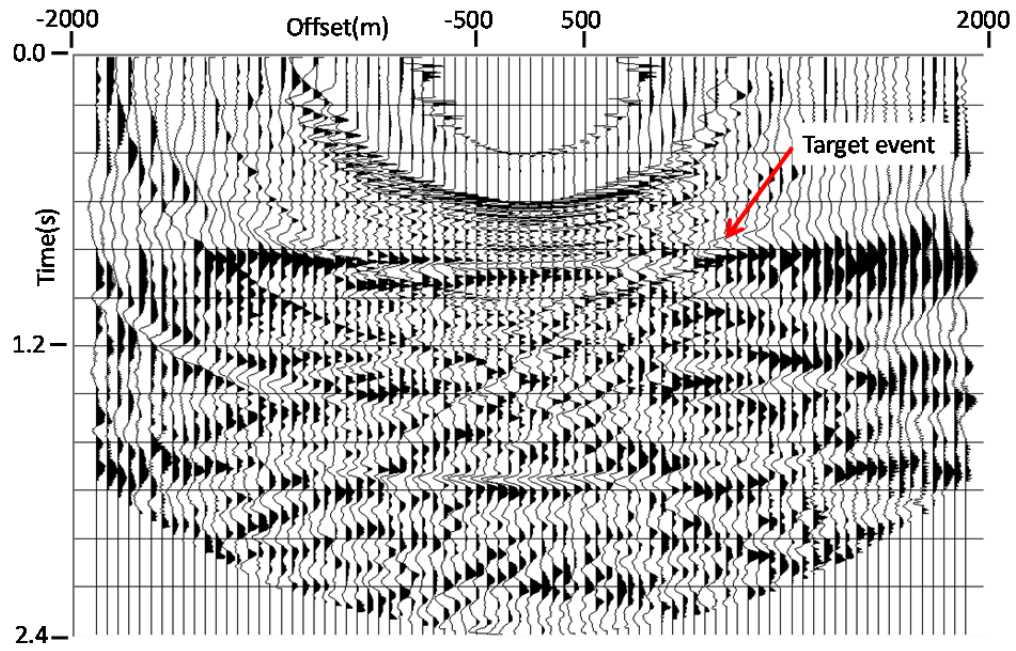


FIG. 29. Time shift and NMO mapping applied to gather in Figure 28.

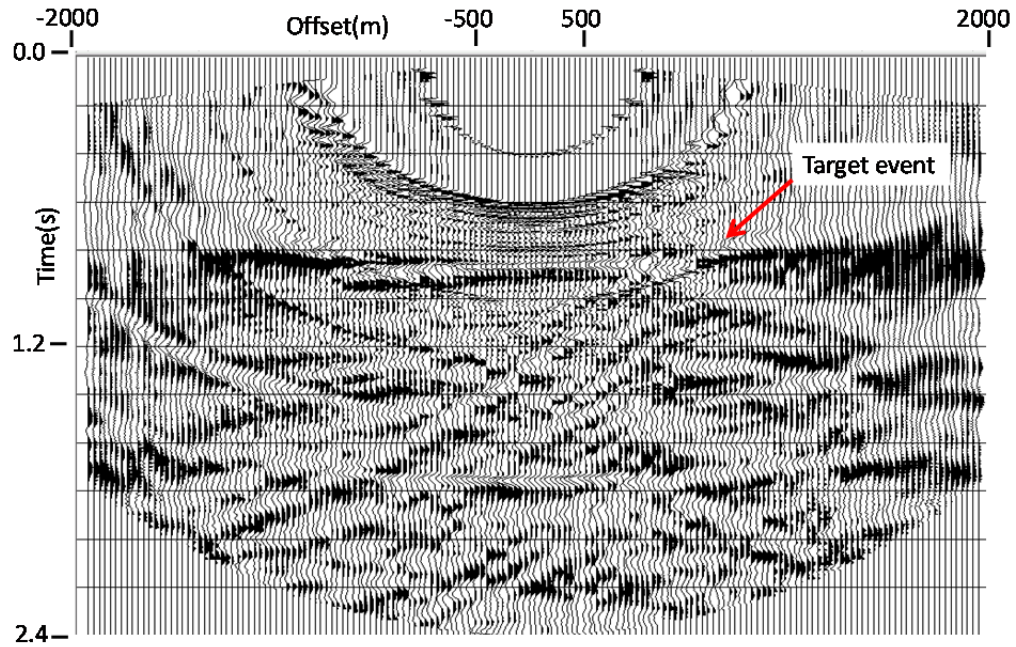


FIG. 30. Radial component source gather interpolated x2.

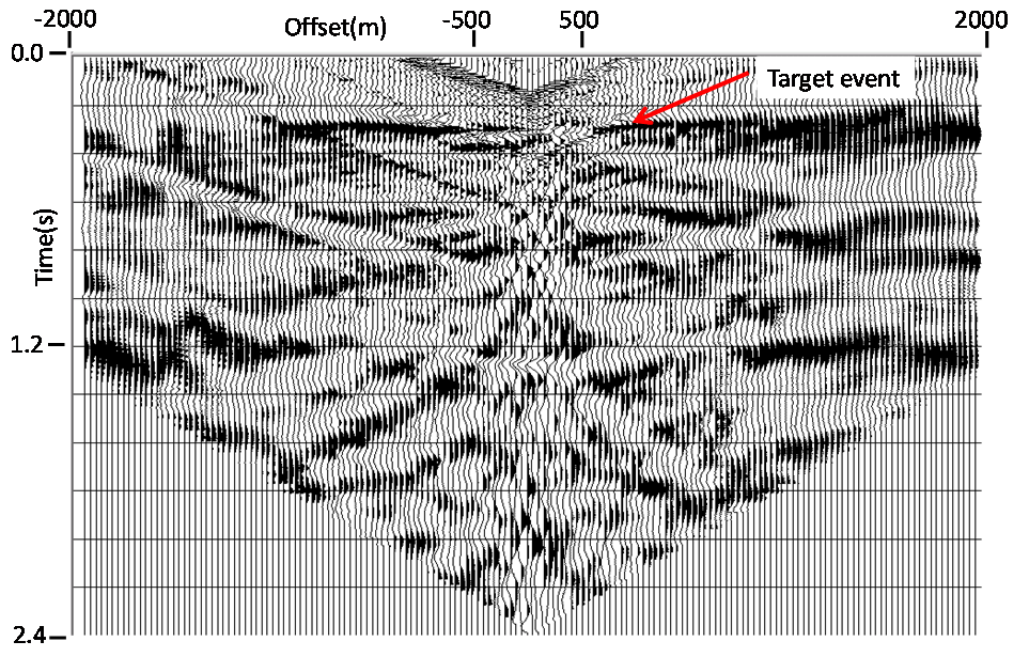


FIG. 31. Source gather mapped to  $T^2-X^2$  domain.

### Isolating the target event

Since the events which interfere with our target event have hyperbolic moveout, we applied the  $T^2-X^2$  transform to linearize the event wavefronts, as in Figure 31. This resulted in a flat target event with several interfering linear events, which are now susceptible to RT dip filtering. We detected a set of such events with apparent velocity (in this domain) of  $\pm 5000\text{m/s}$ , show the  $-5000\text{m/s}$  component in Figure 32, and subtracted it and its companion  $+5000\text{m/s}$  noise estimate in Figure 33. Another linear noise system with apparent velocity of  $\pm 3200\text{m/s}$  (Figure 34) was subtracted in Figure 35. After all dipping linear components were estimated and removed, the result is shown in Figure 36. Inverting the  $T^2-X^2$  transform leads to Figure 37. Because this particular implementation of the  $T^2-X^2$  transform is sparse at the nearest offsets, some of the original traces are lost in this region and must be interpolated to their original offset positions (a more sophisticated implementation could avoid this issue). Inverting the  $T^2-X^2$  transform also caused further aliasing of some of the shallow events; but this is of no concern for the isolation of our target event. Inverting the NMO transform resulted in Figure 38, where the target event is much more easily picked than in the original gather (Figure 28). An alternative processing scheme was tested, in which the  $T^2-X^2$  transform and its inverse were eliminated from the flow, and the events interfering with the target event were removed by a series of RT dip filters directly in the NMO transform domain. Since the interfering events are curved, a larger number of dip filters was required to attenuate them; but the near-offset trace interpolation required in the inverse  $T^2-X^2$  transform is thereby eliminated. The result of this alternate processing flow is shown in Figure 39. Here, we see that the target event is quite comparable in its strength and clarity to that in Figure 38, and that it may actually be easier to pick at the longer offsets.

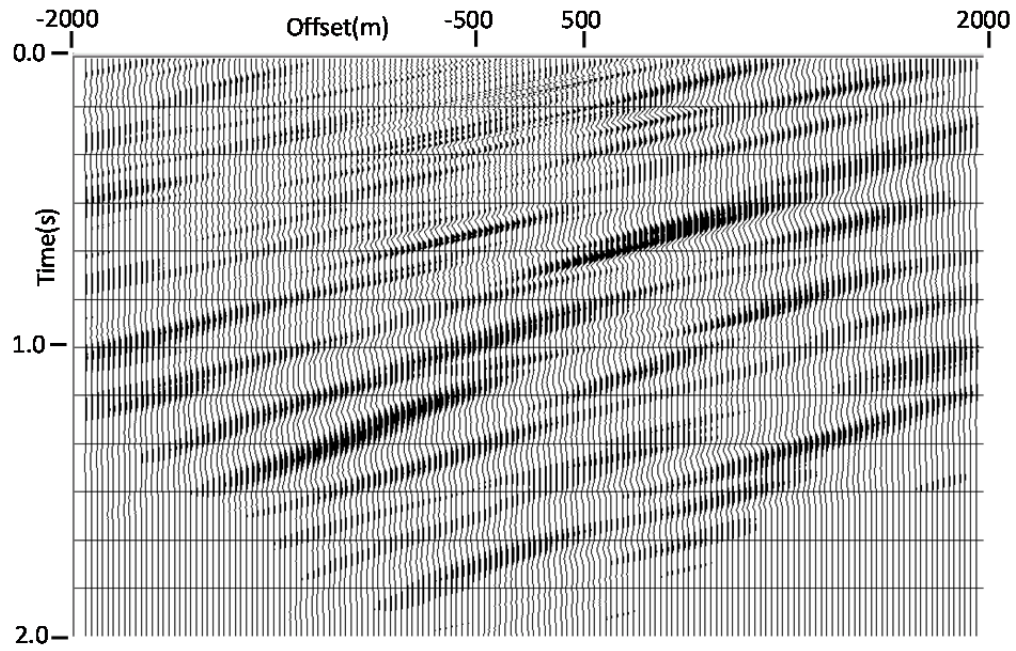


FIG. 32. Linear component estimated using RT dip filter for -5000m/s. Similar component can be estimated for +5000m/s.

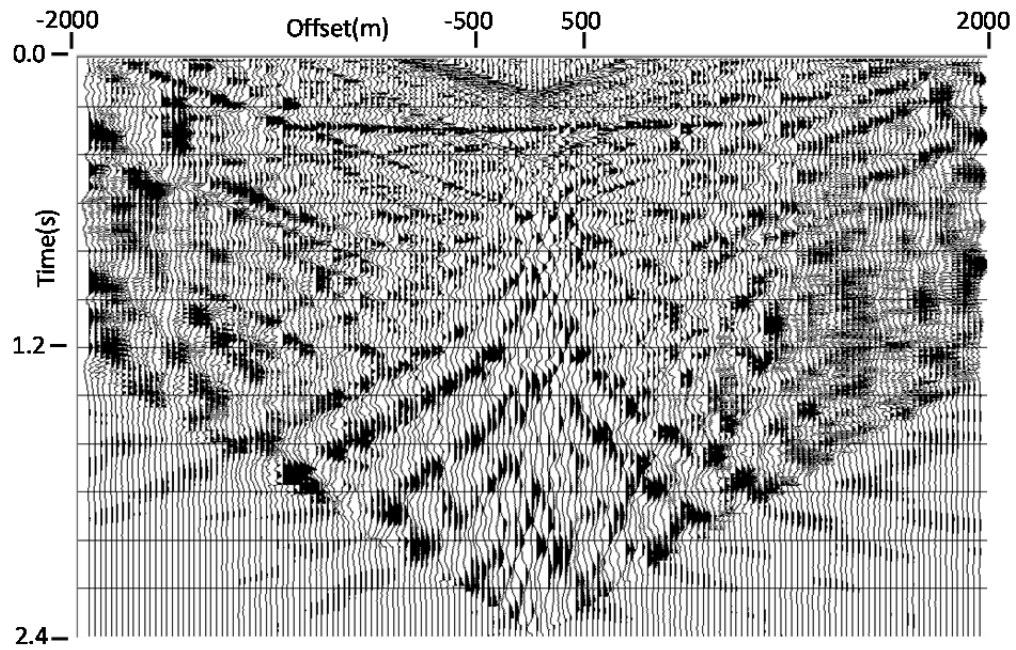


FIG. 33. Linear components at +/- 5000m/s removed from gather.

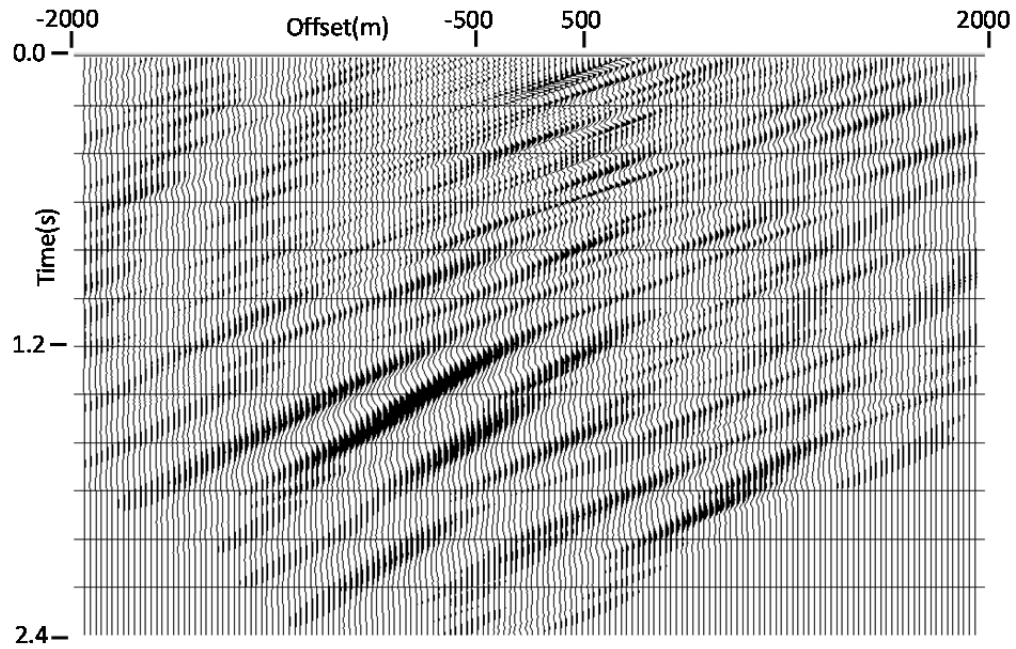


FIG. 34. Linear component estimate for -3200m/s. Similar component can be estimated for +3200m/s.

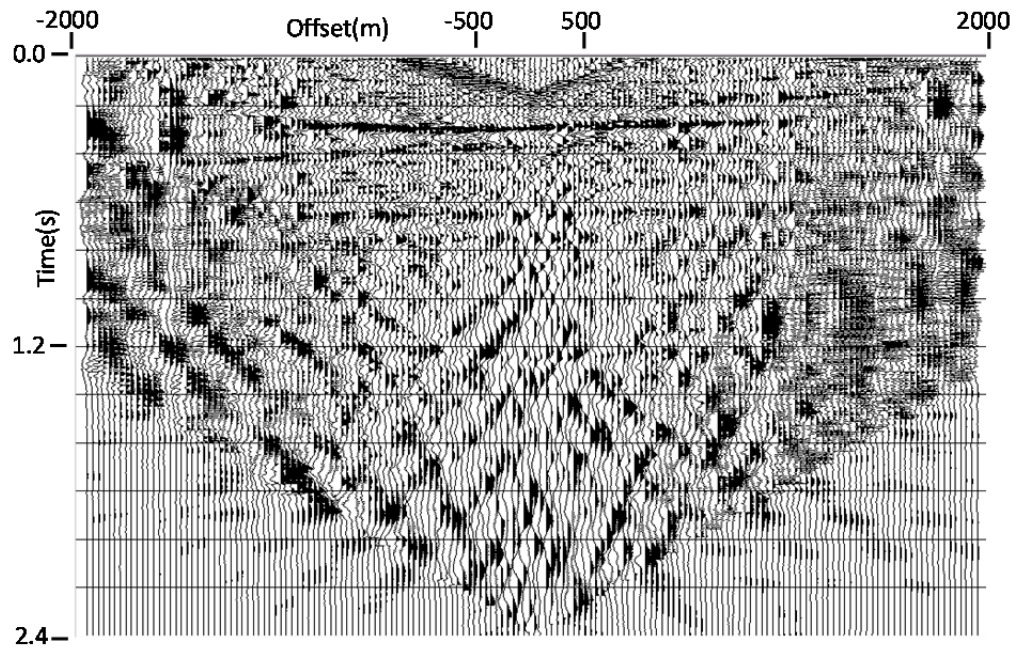


FIG. 35. Linear components at +/- 3200m/s removed from gather.

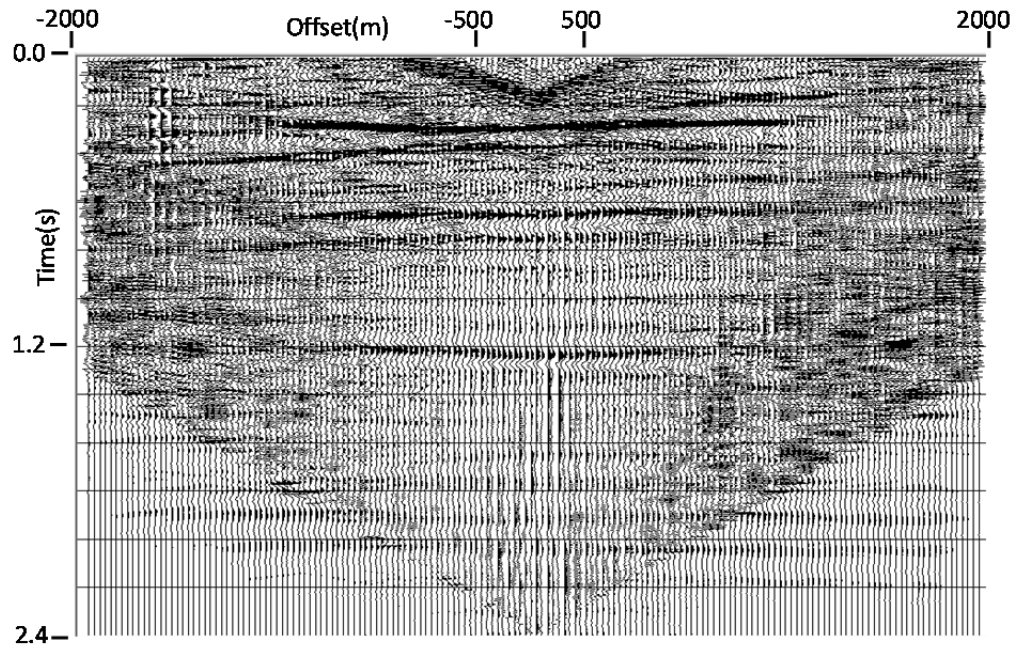


FIG. 36. Several linear components estimated and subtracted from receiver gather.

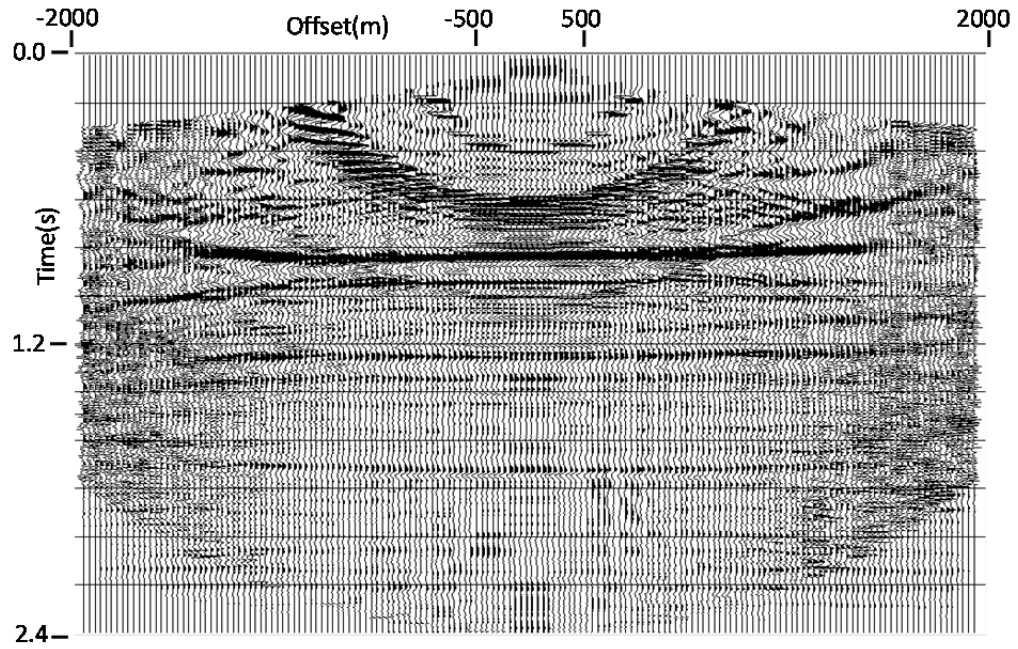


FIG. 37. Radial component gather mapped back to X-T domain.

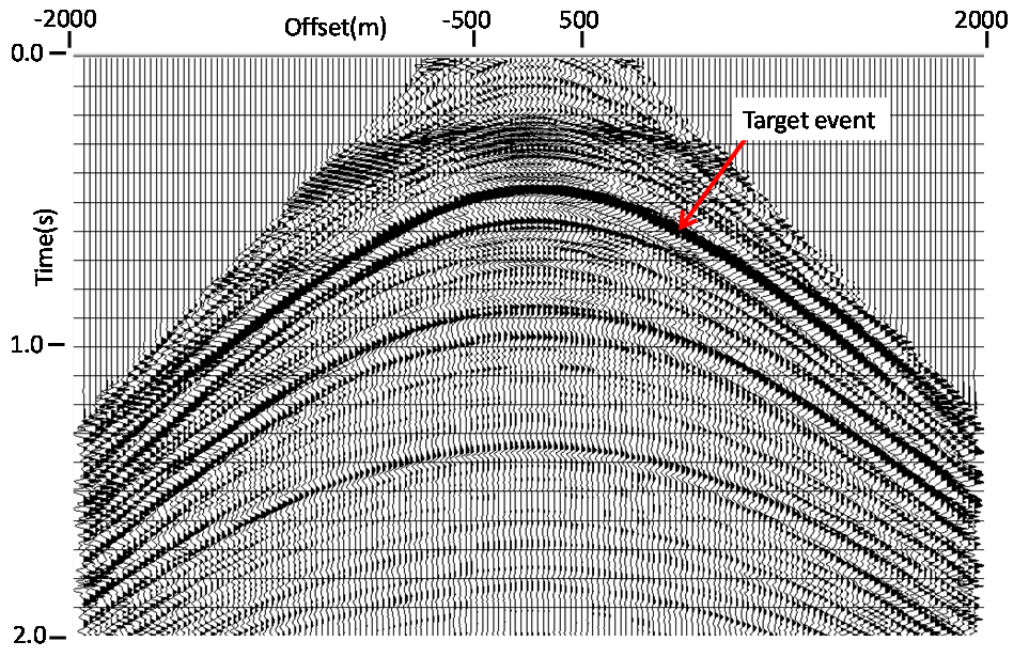


FIG. 38. Inverse NMO mapping of Figure 37. Target event is much clearer than in Figure 28, and could be easily picked for arrival times.

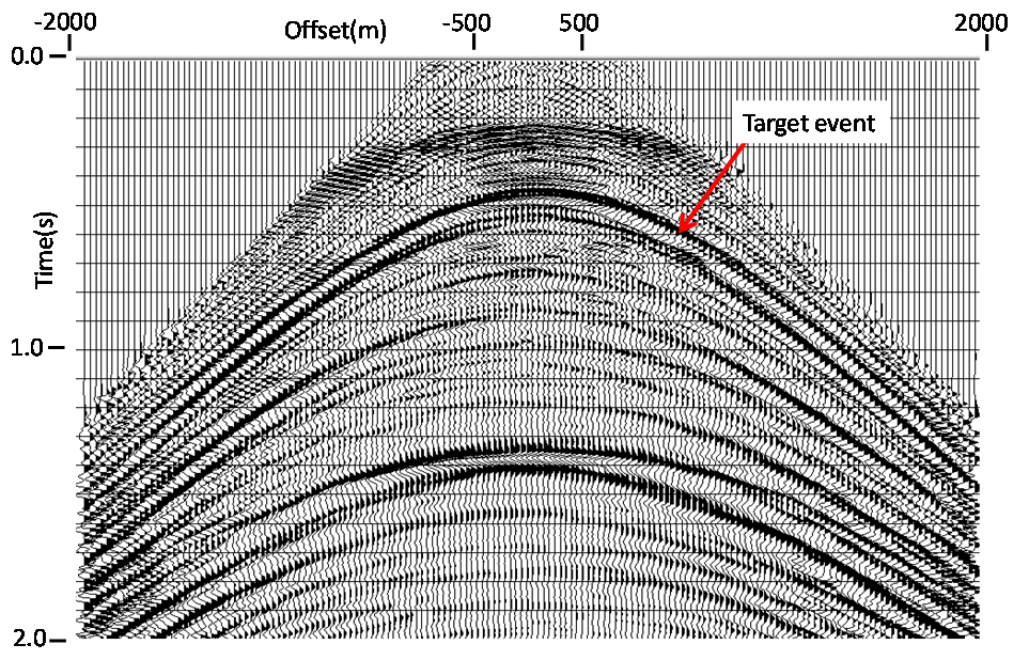


FIG. 39. Alternate processing applied to Figure 28, with no mapping to the  $T^2$ - $X^2$  domain. Target event may be more easily picked than in Figure 37.

## DISCUSSION

We have demonstrated the use of simple geometric distortions of the  $X$ - $T$  plane in which seismic data are usually represented, to facilitate a simple estimation and subtraction strategy for isolating a desired seismic wave mode from a complex wavefield.

The use of such distortions is attractive because they are easily implemented, and done carefully, can be almost exactly inverted, with little loss of information, unlike some integral transform methods. Because they are relatively easily visualized, geometric distortions can add to the intuitive understanding of the data manipulation involved.

The data used in this study were all created using our physical modeling apparatus. This is attractive because we can positively identify the various components of the generated wavefield and control their relative strength and position by selecting the materials and dimensions of the model, as well as the transducer geometry used in surveying the model. In the current study, the model was simple, but contained enough complexity (vertical seams, or ‘faults’) to create a challenging wavefield for our separation attempts.

Since the objective of wavefield separation in many cases is the measurement of amplitudes or travel times of specific events, the separation need not be perfect—but it must increase the S/N of the desired event enough to make the measurements as clean as possible. That has been the objective of the examples shown here.

There are many possible implementations of the mapping transforms demonstrated above, some of which would likely outperform the ones we have used, particularly in the types of interpolation employed.

#### **ACKNOWLEDGEMENTS**

The authors acknowledge CREWES sponsors and NSERC for funding, CREWES staff, and especially Faranak Mahmoudian, for stimulating discussion and use of her model for this demonstration.

#### **REFERENCES**

- Henley, D.C., 2001, More radial trace domain applications, CREWES research report—Volume 12(2000).
- Henley, D.C. 2003, Coherent noise attenuation in the radial trace domain, *Geophysics*, **68**, No. 4, pp1408-1416.
- Henley, D.C., 2011a, Now you see it, now you don’t: radial trace filtering tutorial, CREWES research report—Volume 23(2011).
- Henley, D.C., 2011b, Getting something for nothing—or not: interpolating coherent noise, CREWES research report—Volume 23(2011).
- Mahmoudian, F., Margrave, G.F., Daley, P.F., Wong, J., and Gallant, E., 2010, Determining elastic constants of an orthorhombic material by physical seismic modeling, CREWES research report—Volume 22(2010).
- Mahmoudian, F., Margrave, G.F., Daley, P.F., and Wong, J., 2012a, Estimation of stiffness coefficients of an orthorhombic physical model from group velocity measurements, CREWES research report—Volume 24(2012).
- Mahmoudian, F., Margrave, G.F., and Wong, J., 2012b, Azimuthal AVO over a simulated fractured physical model medium, CREWES research report—Volume 24(2012).